

Citation for published version:

Zhou, S, Chen, K, Cole, M, Li, Z, Li, M, Chen, J, Lienau, C, Li, C & Dai, Q 2021, 'Ultrafast Electron Tunneling Devices—from Electric-field driven to Optical-field driven', *Advanced Materials*, vol. 33, no. 35, 2101449. <https://doi.org/10.1002/adma.202101449>

DOI:

[10.1002/adma.202101449](https://doi.org/10.1002/adma.202101449)

Publication date:

2021

Document Version

Peer reviewed version

[Link to publication](#)

This is the peer reviewed version of the following article: Zhou, S. H., Chen, K., Cole, M. T., Li, Z. J., Li, M., Chen, J., Lienau, C., Li, C., Dai, Q., Ultrafast Electron Tunneling Devices—From Electric-Field Driven to Optical-Field Driven. *Adv. Mater.* 2021, 33, 2101449. which has been published in final form at <https://doi.org/10.1002/adma.202101449>. This article may be used for non-commercial purposes in accordance with Wiley Terms and Conditions for Use of Self-Archived Versions. This article may not be enhanced, enriched or otherwise transformed into a derivative work, without express permission from Wiley or by statutory rights under applicable legislation.

University of Bath

Alternative formats

If you require this document in an alternative format, please contact:
openaccess@bath.ac.uk

General rights

Copyright and moral rights for the publications made accessible in the public portal are retained by the authors and/or other copyright owners and it is a condition of accessing publications that users recognise and abide by the legal requirements associated with these rights.

Take down policy

If you believe that this document breaches copyright please contact us providing details, and we will remove access to the work immediately and investigate your claim.

DOI: 10.1002/ ((please add manuscript number))

Review

Ultrafast Electron Tunneling Devices—from Electric-field driven to Optical-field driven

Shenghan Zhou, Ke Chen, Matthew Thomas Cole, Zhenjun Li, Mo Li, Jun Chen, Christoph Lienau, Chi Li, and Qing Dai**

S. H. Zhou, K. Chen, Dr. Z. J. Li, Prof. C. Li, Prof. Q. Dai

Division of Nanophotonics, CAS Center for Excellence in Nanoscience, National Center for Nanoscience and Technology, Beijing 100190, China

E-mail: lichi@nanoctr.cn; daiq@nanoctr.cn

S. H. Zhou, K. Chen, Dr. Z. J. Li, Prof. C. Li, Prof. Q. Dai

University of Chinese Academy of Sciences, Beijing 100049, P. R. China

Dr. M. T. Cole

Department of Electronic and Electrical Engineering, University of Bath, BA2 7AY, UK

Prof. M. Li

School of Electronic Science and Engineering, University of Electronic Science and Technology of China, Chengdu 611731, China

Prof. J. Chen

State Key Laboratory of Optoelectronic Materials and Technologies, Guangdong Province Key Laboratory of Display Material and Technology, School of Electronics and Information Technology, Sun Yat-sen University, Guangzhou 510275, China

Prof. C. Lienau

Institut für Physik, Center of Interface Science, Carl von Ossietzky Universität, Oldenburg, 26129, Germany

Keywords: electron tunneling device, direct tunneling, resonant tunneling, single-electron tunneling, inelastic tunneling, optical-field-driven

The search for ever higher frequency information processing has become an area of intense research activity within the micro, nano and optoelectronics communities. Compared to conventional semiconductor-based diffusive transport electron devices, electron tunneling

devices provide significantly much faster response time due to near-instantaneous tunneling that occurs on femtosecond time scales. As a result, the enhanced performance of electron tunneling devices has been demonstrated, time and again, to reimagine a wide variety of traditional electronic devices with new “lightwave electronics” emerging capable of reducing the time of electron transport in channel, down to femtosecond, and even attosecond timescale.^[1] In response to unprecedented progress within this field, here the current state-of-the-art in electron tunneling devices is reviewed, current challenges are highlighted, and possible future research directions are identified.

1. Introduction

Microelectronics remain the bedrock of our modern digital age. However, due to continued device miniaturization, modern electronics are experiencing two technologically challenging and functionally significant bottlenecks linked to their speed limitation and high power consumption.^[2] Both challenges are principally linked to electron-phonon interactions during transport in these conventional semiconductor channels. New approaches to device fabrication, capable of supporting alternative modes of electron transport, are urgently required to allow for continued speed improvements whilst concurrently reducing power consumption. Electron tunneling devices represent on class of potential solution that can simultaneously realize ultrafast response at attosecond (10^{-18} s) timescale, low power consumption and miniaturization, which are likely to manifest through the fusion of conventional solid-state electronics and vacuum electronic devices.

Due to the inherently limited switching speed of electronics driving systems, it remains

challenging to breakthrough the picosecond (10^{-12} s) bottleneck of the response time with conventional electrically driven electron tunneling devices. The use of ultrafast lasers for optical-field-driven tunneling devices has established one important way to breakthrough this technologically response time limit.^[3-5] The quantum mechanical tunneling of electrons through a potential barrier involves almost no scattering and negligible energy loss and occurs over sub-optical-cycle frame—attosecond time (10^{-18}) timescale.^[3, 4, 6, 7] Nonlinearity in the ultrafast tunneling process can convert the sub-optical-cycle response into a technologically useful direct current. These optical-field-driven electron tunneling devices have the potential for much wider use in on-chip “lightwave electronics”.^[8-16]

Recently, novel low-dimensional, especially carbon-based nanomaterials, used in electron tunneling devices provided a platform with significant potential for high-speed devices. With rapid advancements in low dimensional materials with tailor-designed band-structures,^[17, 18] a wide variety of emerging tunneling devices have come to the fore, each exhibiting superior performance in contrast to traditional materials with continuous band-structures. It is widely believed that electron tunneling devices, when aligned with the provision of engineered low-dimensional material systems, will drive a more-than-Moore future, allowing for the development of new and functionally novel nano-electronic architectures capable of high-speed and low-power consumption.

Here, we summarize the present state-of-the-art in this emerging and rapidly evolving field. We first review the operation principles of electric-field-driven tunneling and optical-field-driven tunneling based on different tunneling mechanisms, including direct tunneling, resonant tunneling, and inelastic tunneling. Then, we discuss current developments of electric-field-

driven electron tunneling devices, focusing on the materials and device architectures. Finally, we provide an outline of some of the most recent demonstrations of optical-field-driven tunneling devices and some brief outlooks into the future directions of this field.

2. Principles of electron tunneling

In this section, the operation principles of electric-field-driven tunneling and optical-field-driven tunneling are summarized, including direct tunneling, resonant tunneling and inelastic tunneling.

2.1 Electric-field-driven tunneling

2.1.1 Direct tunneling

Metal-insulator-metal (MIM) multi-layer structures are one of the most structurally simple, and hence most widely investigated, types of tunneling devices. The band diagram of a typical direct tunneling MIM structure is shown in **Figure 1a**. Here, the electrons from the surface of the left metal can tunnel directly through the energy barrier formed by the dielectric layer. For thick dielectrics, direct tunneling is little noticed in the transport profile, direct tunneling dominates electron transport as the dielectric layer gets increasingly thin, especially for sub-10-nm dielectrics. With research spanning more than four decades, MIM devices are comparatively mature technology. MIMs find use mainly in electronic components such as double-gate tunneling field-effect transistors (FET) and high-k gate dielectric tunneling FETs.^[19, 20] Though capable of being modeled by a wide range of transport models, that depend critically on a variety of material and device structural properties, the Fowler-Nordheim (F-N) tunneling model is perhaps the most commonly used model for direct tunneling. As depicted in **Figure**

1b, in the F-N model the electrons do not tunnel directly to the other side of the barrier. Rather, they tunnel from the surface of the left metal to the conduction band of the insulator. The F-N tunneling regime is significant for thicker dielectrics and sufficiently high electric fields. In the case when the dielectric is a vacuum, a metal-vacuum-metal (MVM) structure is formed. The exploration of these nanoscale vacuum-channel diodes (NVD) is another recently hot research topic.^[21-26] NVDs inherit many of the functional advantages of traditional, often bulky vacuum electronic devices, such as high operation frequency and high output power, as well as many of the production benefits associated with conventional silicon integrated circuitry. NVDs are well-positioned to capitalize on the merits of both established communities, particularly as the channel length becomes less than the electrons mean free path in air, the technologically demanding and bulky vacuum environments in traditional device becomes unnecessary supporting the realization of air-operation devices.

2.1.2 Resonant tunneling

Since the 1970s, resonant tunneling devices have attracted significant attention for their use in radio frequency oscillators, multi-valued logic, high-frequency radar, communication systems, and signal processing.^[27-32] **Figure 1c** shows a typical energy band diagram of a resonant tunneling device. When a bias voltage V_b is applied for which the Fermi level E_c of the top electrode matches the quantum well energy level E_0 , resonant tunneling can be established and a local maximum in the conductance occurs, evidenced in the measured current-voltage (I-V) profiles. Resonant tunneling of charge carriers between two spatially separated quantum states can lead to negative differential resistance (NDR),^[33, 34] which is a key feature for novel nanoelectronic circuits. In addition, high currents can be achieved at low voltages

through clever band engineering in resonant tunneling devices due to the excellent energy level control ability of quantum well.

Single-electron tunneling is a special case of resonant tunneling where the electrons are transported one by one through a quantum dot (QD). Single-electron tunneling devices operate via a capacitive charging energy (i.e., classical Coulomb blockade effect), which makes it possible to inject controllably, at well-defined energies, single carriers into quantum dots. Single-electron tunneling devices have garnered great attention because of their concurrent high-speed and low-power operation, and specifically for their potential deployment in emerging qubit applications.^[35-38] **Figure 1d** shows a typical energy band diagram of a single-electron tunneling device. When the Fermi level of the top electrode matches the QD energy level, only one electron can tunnel into the unoccupied levels of the QD from the top electrode through the barrier. This electron then tunnels into the bottom electrode when the Fermi level of the bottom electrode is equal to the QD energy level. This electrical characteristic of the single-electron tunneling phenomenon has been extensively characterized and is well described based on the double-barrier tunneling junction (DBTJ).^[39, 40]

2.1.3 Inelastic tunneling

Electrons commonly interact with various quasi-particles, such as phonons, plasmons, and magnons, particularly in solid-channel devices, such as MIMs. In these processes, inelastic tunneling channels may open, usually accompanied by energy loss, and photons may be generated. Inelastic tunneling has been used widely in materials characterization as well as, more recently, in signal generation, transmission, modulation, and detection in photonic integrated devices.^[41-50] **Figure 1e** shows an energy band diagram of an electric-field-driven

inelastic tunneling device in specific case of photon emission. When biased, the electrons tunnel through the barrier layer to another metal electrode in a process that results in stimulated photon emission. The tunneling current includes contributions from both elastic and inelastic electrons. The majority of the electrons tunnel elastically without energy loss. The remaining electrons, a significantly smaller proportion inelastically tunnel through the barrier and lose energy such that $\hbar\omega \leq eV_b$, where \hbar is the reduced Planck constant, ω is the angular frequency of the optical mode and V_b is a bias voltage.^[51] This energy loss excites localized plasmon modes, often termed ‘gap plasmons’.^[52, 53] These plasmons decay through various relaxation pathways, including radiative or non-radiative mechanisms which allow device engineers to create novel device architectures that draw function from these non-ideal transport modes.

2.2 Optical-field-driven tunneling

The underlying mechanism of optical-induced tunneling includes thermal-induced tunneling^[54, 55] and photo-induced tunneling.^[56] Under these regimes, electrons are first excited from their original energy level to a higher energy-level state by absorbing thermal (thermally induced tunneling) or one photon energy (single-photon tunneling). They then face a much narrower tunneling barrier, which results in a highly enhanced emission current. However, such excitation methodologies do not all femtosecond response time. Ultrafast femtosecond laser-assisted electron tunneling is considered the primary candidate method for reaching femtosecond and even attosecond response time. As shown in **Figure 2**, upon illumination with an intense ultrafast laser pulse an electron may emit through the barrier in two ways. First, as shown in **Figure 2a**, electrons in the Fermi level may absorb more than one photon and gain sufficient energy to overcome the barrier height. This is commonly referred to as multi-photon

tunneling.^[57] Here, the electron yield follows an N^{th} power of the laser intensity, where N is the nonlinear order in the absorption processes. The time scale for the multiphoton photoemission follows the width of the laser pulse divided by $N^{1/2}$. Under the influence of a stronger laser field, moving beyond the multiphoton regime, the barrier allows penetration, and subsequent tunneling emission, only in a short period of each cycle of the laser pulse.^[58] In this strong optical-field regime, the time duration of generated electron wavepackets consists of a series of bunches, separated by the cycle period and each shorter than half-cycle of the incident field, as shown in **Figure 2b**. In particular, the use of an ultrafast few-cycled laser can generate tunneling electron wavepackets of sub-femtosecond time duration,^[3-5, 7] which is the basis for achieving attosecond electron transport in nanoscale channels. Photoemission may transition into optical-field emission from the multiphoton emission regime with increasing optical field strength. This transition can be described by the Keldysh framework.^[59] The Keldysh framework introduces a characteristic parameter γ that separates the two photoemission regimes, a multiphoton emission regime^[60] ($\gamma \geq 1$) and a strong optical-field tunneling emission regime^[61] ($\gamma \leq 1$). The Keldysh parameter $\gamma = \omega\sqrt{2m\phi}/e\beta F$, where ω is the optical-frequency; ϕ is the barrier height; m and e are the mass and charge of the electron, respectively; F is the incident light-field strength; β is the field-enhancement factor of the emitter.

According to established strong-field physics,^[3, 4] following the optical-field-driven tunneling process, the electrons are accelerated by the strong optical-field in the near-field of the emitting surface. Hommelhoff et al.^[3] demonstrated carrier-envelope phase (CEP) sensitive high-order photoelectron emission from a W nanotip, with a current modulation of up to 100%. The highly nonlinear phenomenon is attributed to the interference of electron wavepackets that

are coherently emitted during two adjacent optical-cycles. Ropers et al.^[4] observed sub-optical-cycle acceleration in an Au nanotip; a novel form of quiver-quenched electron motion in the strong optical-field regime. Lienau et al.^[5] clarified, for the first time, the effect of the optical-fields CEP on the generation and motion of strong-field-emitted electrons from sharp Au tips. Such field-driven control of electron motion in solid-state nanostructures will pave the way towards new approaches for the generation, measurement and application of attosecond electron pulses. For a recent overview, we refer the reader to reference.^[61, 62] However, optical-field-driven electron dynamics in nanoscale transport volumes remain unclear with much research required, to lay much needed foundations for a new generation of lightwave electronic devices.

3 Recent developments of electric-field-driven tunneling devices

3.1 Direct tunneling devices

In this section, we summarize recent developments in MIM and MVM devices in the direct tunneling regime.

3.1.1 Direct tunneling devices based on traditional materials

Direct tunneling devices can be divided into bipolar (diodes, formed from two sharp tips),^[25] or tertiary (triodes) structures that include additional side^[26] or bottom-gates.^[24, 63] The primary advantage of triodes is their ability to finely control the emission by adjustment of the gate voltage. When the gate voltage is less than the turn-on voltage, a small proportion of the electron population is emitted over the barrier due to thermal excitation linked to the energy spread of the electron populations; the emitted current, however, remains low. As the gate voltage

increases beyond the turn-on voltage, the vacuum energy level bends downward, thus enabling an increasing number of electrons to tunnel through the narrowed potential barrier leading to a dramatic increase in current as soon as the device enters its high-current, low-resistance on-state. In 2012, Meyyappan et al.^[24] demonstrated a planar back-gate FET whose cut-off frequency was 0.46 THz, 10 times greater than comparable semiconductor devices. They predicted that this tunneling structure can potentially improve the cut-off frequency well into the THz regime by process and layout refinements, which, in part, continue to drive the rapid expansion of research on tunneling electronic devices. Nevertheless, non-negligible current leakage to triode gates has proven a long-standing issue.^[24, 26] Recently, to reduce gate leakage current and improve device performance, the same team demonstrated a tunneling transistor consisting of an atomically sharp source and drain electrode embedded in a nanoscale surrounding gate.^[16, 22, 23] **Figure 3a** shows the structure of a typical surround-gate electron tunneling device. The gate leakage current was 10^6 times smaller than the drain current, confirming that the surround-gate dielectric effectively inhibits leakage.

Recently, Sriram et al.^[21] demonstrated a new metal-based nanoscale air-channel tunneling device. They systematically studied the electron emission mechanisms and characteristics of three different tunneling electrodes, namely, tungsten (W), gold (Au), and Platinum (Pt). An optical image and schematic illustration of this air-channel tunneling device are shown in **Figure 3b** and **Figure 3c**, respectively. Due to different work functions and device geometry, the emission in W and Au is fitted with F-N tunneling, whereas the emission is more Schottky-like in the Pt case. Such metal-based tunneling electronic devices provide a platform for future nano vacuum electronics and have the potential to provide a technology basis for low-power,

high-performance applications. Nevertheless, it remains difficult for metal-based nanoscale air-channels to be fabricated through conventional silicon-foundry-based parallel processes that ultimately support high areal device densities that are manufactured with high production yields. Achieving atomically flat metallic interfaces that retain lattice stability has proven particularly challenging to date.^[64-66] Without such ultra-precise surface control, it is believed that further increases in cut-off frequency and power consumption remain limited. This has, in part, driven the search for new materials.

3.1.2 Direct tunneling devices based on low-dimensional nanomaterials

Low-dimensional nanomaterials, and in particular nanocarbon-based materials (such as carbon nanotubes (CNTs) and graphene), have experienced significant interest for their application in electron tunneling applications.^[67-71] Their atomic-scale thickness, ability to self-assemble and unique topologies provide extremely high aspect ratios and thus very high field-enhancement factors that are not attainable by conventional materials and traditional processing either through direct growth or etching. Of the wide range of nanowires discovered and synthesized to date, CNTs have perhaps attracted by far the most attention for use in electron emission systems.^[72-74] The electron emission characteristics of a wide variety of CNT types have been studied, including investigations of electric-field driven,^[75, 76] thermally driven,^[54, 55] and more recently by strong optical-driven.^[72, 73] CNTs have been identified as near-ideal field electron emitters. They have, as a result, been widely used in the fabrication of electron tunneling devices over the past two decades. Maruyama and co-workers^[77] developed a single CNT tunneling device that demonstrated F-N-like tunneling features^[78, 79]. This work was successful in demonstrating the potential of such nanomaterials in simplifying nanoscale

tunneling channel fabrication, whilst also highlighting the opportunity to capitalize on the self-assembly of nanomaterials to grow nano-channels, en masse in highly parallelized processes that are necessary to realize new device architectures.

As a planar 2D material with single-atom thickness, graphene supports high aspect ratio edge emission. Moreover, it can be structured using more conventional thin film processing techniques, whilst retaining the benefits of its atomic thickness. Extensive theoretical and experimental efforts have demonstrated that graphene can be used effectively in tunneling devices, for both planar^[80-84] and vertical structures.^[85-91] Mishchenko et al.^[90] reported on a new vertical tunneling FET based on graphene-WS₂ heterostructures, where WS₂ served as an atomically thin barrier between two layers of graphene (**Figure 3e**). **Figure 3d** shows an optical image of this device. Capable of achieving an on/off ratio $>10^6$, these devices were shown, for the first time, to operate effectively on optically transparent and mechanically flexible substrates. In addition, vertical graphene-based hot electron tunneling transistors from Lemme et al.^[88] have also attracted interest (**Figure 3f**). When a positive voltage is applied to the graphene base electrode, hot electrons tunnel across the lowered barrier of the emitter-base insulator from the conduction band of the n-doped silicon to the base and adopt F-N-like transport. Similarly, Wang et al.^[87] demonstrated a vertical graphene-based hot electron tunneling transistor (**Figure 3g**) where n-doped silicon, graphene, and aluminum were used as the emitter, base, and collector, respectively. A SiO₂ layer served as the tunneling barrier and an Al₂O₃ layer as the filtering barrier. This graphene-based transistor had high effective gain (4.8%), short transit time (picoseconds), and high current on/off ratio ($>10^5$), suggesting potential applications in future high-speed electronics. Most recently, Chen et al.^[91]

demonstrated vacuum electron emission under both directions of bias from a vertical Gr/h-BN based heterostructure (**Figure 3h**), which not only expand the understanding of hot carrier scattering process in graphene but also provide insights into the applications of hot carrier devices.

In addition to graphene, some other two-dimensional materials are also used in electron tunneling devices to improve the cut-off frequency. Most recently, Akinwande et al.^[15] demonstrated that hexagonal boron nitride (h-BN) configured in a metal-insulator-metal (MIM) on a diamond substrate can be used as an analogue switch for applications in communication systems across radio, 5G and THz frequencies. **Figure 3i** shows the MIM tunneling structure of a monolayer h-BN radio-frequency (RF) switch fabricated on a polycrystalline diamond substrate. These devices showed a low insertion loss (≤ 0.5 dB), high isolation (up to 200 GHz), and a calculated cut-off frequency of 129 THz due to their nanoscale vertical and lateral dimensions. They offer a low resistance in the on-state and low capacitance in the off-state, metrics that are superior to those of existing solid-state switches. Such MIM-based tunneling devices could lead to the development of nanoscale energy-efficient high-frequency solid-state switch technology for rapidly growing communication systems in the 5G band and beyond.

3.2 Resonant tunneling devices

3.2.1 Resonant devices based on traditional materials

Conventional resonant tunneling devices comprising a quantum well sandwiched between two tunnel barriers that are typically tens of nanometers thick and commonly fabricated from Si/SiGe,^[92-94] or III-V quantum well systems,^[95-97] although other conventional material systems have also been used.^[98, 99] Similarly, single-electron tunneling devices have also been

realized with various traditional materials, including Si QDs,^[100, 101] metal nanoparticles,^[102, 103] single molecules,^[104, 105] topological insulators,^[106] and other QDs.^[107, 108] Hiramoto et al.^[101] reported on the observation of multiple large quantum-level splitting with extreme charge stability in a Si single-electron transistor (SET) at room temperature. The structure of this device is shown in **Figure 4a**. The device is fabricated from a Si nanowire-channel metal–oxide–semiconductor field-effect transistor (MOSFET), where the Si QD and the tunnel barriers are self-formed by a volumetric undulation process. Recently, Pistolesi et al.^[105] theoretically investigated single-photon emission mediated by molecule-based single-electron tunneling devices. **Figure 4b** shows the schematic of two metallic electrodes forming a plasmonic nanocavity, characterized by a resonance frequency $\omega_c/2\pi$ and a damping rate κ . A single electronic level ε_0 of a molecule in the nanogap couples to the electromagnetic radiation with coupling constant Λ_m . Electrons can tunnel to and from the dot with tunneling rates Γ_α . So far, despite intensive research efforts exploring a range of different material systems, the obtained performance of the integrated resonant tunneling devices (such as peak-to-valley ratio, response frequency) has been limited.

3.2.2 Resonant tunneling devices based on low-dimensional nanomaterials

Atomically flat interfaces and sharp energy band edges are desirable for the development of tunneling devices.^[109, 110] Two-dimensional van der Waals (vdWs) heterostructures can thus provide unique opportunities for future device design.^[111–115] Multilayer stacks of graphene and other atmospherically stable, atomically thin, two-dimensional materials such as boron nitride, the metallic dichalcogenides, MXenes, and layered oxides^[116] offer the prospect of the potential creation of a new class of engineered tunneling heterostructure materials. In these structures,

different 2D materials and thin insulators can be stacked, often without lattice mismatch and associated band bending constraints, due to the weak vdWs interaction between layers. The increasing availability of numerous different 2D materials—with a variety of different band structures, from semi-metals to semiconductors to insulators—makes it possible to assemble unique materials with engineered band alignments.^[109, 110, 117, 118]

The combination of an h-BN barrier layer sandwiched between two graphene electrodes is particularly attractive and has been widely studied during the last decade,^[119-122] because of the exceptional crystalline quality, the excellent transport properties, and the small lattice mismatch, reducing band bending caused by lattice strain, of these two materials. As shown in **Figure 4c**, Novoselov et al.^[121] demonstrated a resonant tunneling graphene-hBN transistor, which employed h-BN as the barrier layer^[123] between two graphene electrodes. A tunneling current was generated by the application of a bias voltage, V_b , between the bottom and top graphene electrodes. The gate voltage, V_g , was applied between the doped silicon substrate and the bottom electrode. Resonance occurs when the energy band of the two electrodes are aligned. The tunneling current is exponentially dependent on the h-BN barrier thickness, supporting the speculated quantum transport model. An unprecedented degree of control over the electronic properties is available not only by means of the selection of materials in the stack,^[124] but also through the additional fine-tuning achievable by adjusting the built-in strain and relative orientation/rotation of the component layers.^[125-129] By aligning the crystallographic orientation of the two graphene layers in the graphene/h-BN/graphene heterostructure, the same team demonstrated that this device can achieve resonant tunneling with conservation of electron energy, momentum, and, potentially, chirality.^[122] **Figure 4d** depicts the schematic of this

resonant tunneling transistor with an exaggerated angle θ between two graphene layers (separated by an h-BN tunnel barrier shown in light blue). The heterostructure is placed on a SiO_x/Si substrate (magenta/light grey), which serves as an electrostatic gate. These resonant tunneling devices are free of the fundamental limitation intrinsic to conventional double-barrier resonant tunneling devices, namely the relatively long carrier dwell time (picoseconds) in the quantum well as compared with the time to transit the barrier (femtoseconds). Therefore, such tunnel circuits have extraordinary potential in shaping future high-speed electronic devices.

Most recently, Kim et al.^[130] demonstrated the simultaneous use of graphene-based in-plane and vdWs heterostructures to build vertical SETs. As shown in **Figure 4e**, graphene QDs are grown inside a matrix of h-BN, which dramatically reduces the number of localized states along the perimeter of the QDs. The use of h-BN tunnel barriers as contacts to the graphene QDs make SETs reproducible and independent of localized states, which open up many opportunities in the design of future devices.

Other layered nanomaterials are also used in resonant tunneling devices. Most recently, Wu et al.^[131] reported a tunneling field-effect transistor made from a black phosphorus (BP)/ Al_2O_3 /black phosphorus vdWs heterostructure in which the tunneling current was in the transverse direction with respect to the drive current. A schematic of the device is shown in **Figure 4f**. The top BP layer is p-doped while the bottom BP layer is n-doped. There is a remarkable NDR behavior, showing an abrupt decrease in drain current for a small change in drain voltage. In this NDR region, the drain current is more than 10^3 times larger than the gate leakage current I_g or collector current I_c . This is fundamentally different from conventional tunneling devices where the tunneling current typically equals the change in drain current.

Through an electrostatic effect, this tunneling current can induce a dramatic change in the output current, leading to a tunable NDR with a peak-to-valley ratio > 100 at room temperature.

With continued research into new 2D materials and new vdWs heterostructures, it is becoming more widely accepted that a variety of new and important applications have and will continue to emerge, including novel photodetectors,^[97] evaporative electron cooling,^[132] and resonant tunneling spectroscopy,^[133] all of which further highlight the continuing technological value of new resonant tunneling devices.

3.3 Inelastic tunneling devices

In this section, we focus on the emission of a photon and gap plasmons, which is a specific case of inelastic tunneling. One of the most attractive applications of inelastic tunneling devices perhaps lies in the realization of nanoscale light sources. Inelastic electrically excited spontaneous radiation through a tunnel junction was first observed in a MIM structure in 1976 by Lambe and McCarthy.^[134] This emission is a two-step process. A gap plasmon is first excited in the MIM junction. Then, this gap plasmon leads to light emission by either decaying directly into a photon or by coupling to a surface plasmon.^[51, 135, 136] Such optical sources can confine light to the nanoscale through interface resonance effects.^[137] Generally, the low generation ratio of inelastic electrons restricts the electron-to-plasmon conversion efficiency ($< 10\%$). The plasmon-to-photon conversion efficiency is also similarly extremely low ($< 0.1\%$) due to wave-vector mismatch.^[41] These adverse factors lead to comparatively low light emission efficiency (10^{-3} - $10^{-2}\%$) that make practical applications of such nanoscale light sources difficult.^[42] Nevertheless, local optical hot spots introduced by surface plasmon resonances have been shown to enhance the electron-to-photon conversion efficiency by a factor of 10^2 , resulting in

potentially functionally viable light emission efficiencies of around 2%.^[42, 138, 139] Tunneling junctions with integrated optical antennas efficiently bridge the size mismatch between nanoscale volumes and far-field radiation and in doing so are one approach towards dramatically enhancing the electron-photon conversion efficiency. Electron tunneling structures have been shown to support electric-field-driven light generation via inelastic tunneling in metal-insulator-semiconductor (MIS)^[140, 141] and MIM^[41-43] tunneling junctions, with much ongoing research exploring the use of these structures in more advanced architectures.

3.3.1 Inelastic tunneling devices based on traditional materials

An electric-field-driven optical antenna was first demonstrated by Hecht et al.^[43] in 2015. An electron micrograph of this lateral tunneling structure is shown in **Figure 5a**. Subsequent to this, Novotny et al.^[41] demonstrated an antenna-coupled MIM tunneling junction, as shown in **Figure 5b**. These tunneling junctions consisted of a vertical stack of segmented, nanostructured Au bottom electrodes, few-layer h-BN and a common Au top electrode. The emission originates from inelastic electron tunneling in which the energy is transferred to surface plasmon polaritons (SPPs) and subsequently converted to far-field radiation by an optical antenna (inset of **Figure 5b**). It was found that the spectrum of the emitted photons was determined by the antenna geometry and can be readily tuned via the application of a voltage to the antenna. It was observed that the direction and polarization of the light emission can be controlled by engineering the antenna resonance, which has the added benefit of improving the external quantum efficiency by approximately two orders of magnitude.^[43] Nijhuis et al.^[44] demonstrated a MIM tunneling junction in an on-chip electronic-plasmonic transducer with an effective efficiency of ~14%. This ultra-compact device integrated light emission and detection

on a single chip. **Figure 5c** shows how the two MIM tunneling junctions are plasmonically coupled via their Au leads, which serve as the plasmonic waveguide. Later, Liu et al.^[42] reported on a Ag nanoantenna tunnel junction with a large local density of optical states (LDOS) in the tunneling nanogap. This structure was shown to increase the far-field light emission efficiency from ~0.01% to ~2%. This inelastic tunneling device is schematically illustrated in **Figure 5d**. Here, photons are emitted from an electronically biased junction formed by two Ag nanocrystals. Such inelastic electron tunneling devices have significant potential in the ultrafast conversion of electrical signals to optical signals at the nanoscale, which can be used in integrated electric-field-driven light sources with controlled emission frequencies for potentially technologically disruptive high-speed on-chip interconnection applications.

Recently, inelastic electron tunneling devices were explored for new applications in chemical catalysis.^[45] **Figure 5e** shows the device configuration of electrically driven plasmonic nanorod metamaterials based on metal-air-metal tunneling junctions using liquid eutectic gallium indium (EGaIn) as a top contact. The majority of the electrons tunnel elastically to form hot electrons in the Au nanorod tips; the inelastically-tunneling electrons excite surface plasmons in the metamaterial, which then decay non-radiatively via the excitation of hot carriers or radiatively into photons from the substrate side of the metamaterial. By monitoring either the changes in the tunneling current or the light intensity due to radiation of the excited plasmonic modes, the reactive tunnel junctions have the potential to control chemical reactions at the nanoscale.

3.3.2 Inelastic tunneling devices based on low-dimensional nanomaterials

Besides metal-based tunneling structures, a variety of novel nanocarbon materials have been used in a range of inelastic tunneling devices. Graphene-based inelastic tunneling devices have shown considerable promise due to the linear dispersion of their Dirac cone, a tunable Fermi level, and nearly flat absorption profile.^[142-144] Koester et al.^[49] reported on an ultrasmall (< 100 nm) plasmonic single nanoparticle light source driven by a graphene tunneling junction. A schematic of the device structure and the light emission mechanism is shown in **Figure 5f**. A gap plasmon is formed between a base Au electrode and a single Au nanoparticle separated by a thin (<10 nm) dielectric gap. This gap mode is electrically excited by electrons inelastically tunneling from the base electrode, through a thin Al₂O₃ dielectric, and into a graphene layer located underneath the nanoparticle. Graphene acts as an ultrathin transparent counter electrode for tunneling while minimizing disruption of the plasmon mode. Novotny et al.^[50] demonstrated light emission from van der Waals quantum tunneling (vdWQT) devices. These devices comprise a vertical stack of Ag, h-BN and graphene, as illustrated in **Figure 5g**. Applying a voltage V_b across the insulating few-layer h-BN crystal results in antenna-mediated photon emission. Photon emission from inelastic electron tunneling can be locally enhanced by coupling to an optical antenna. This can achieve resonant enhancement of the photon emission rate in narrow frequency bands (full width at half maximum of ~57 meV) by four orders of magnitude. Nanocube antennas provide a high local density of states (LDOS) and give rise to a narrow emission spectrum. In this device configuration, the electronic LDOS is controlled by the hybrid vdWs heterostructure whereas the optical LDOS is governed by the nanocube antenna. The optical mode confinement in these vdWQT devices can be defined independently

of the electrical tunnel junction—establishing a new paradigm in nanoscale optoelectronic interfacing.

Advances in nanocarbon-based science during the last decade have driven a recent explosion of new materials that provide an unprecedented variety of novel transport mechanisms which has served to accelerate research in the tunneling devices community. Clearly, direct tunneling devices have demonstrated far-reaching potential as the physical basis for achieving high-speed electronic devices in a variety of technologies. Much work, however, remains to be undertaken to improve the existing devices and to develop new concepts for devices with radically enhanced efficiency and speed.

4 Optical-field-driven electron tunneling devices

The time that it takes for electrons to directly tunnel through a barrier with nanoscale thickness has been intensely discussed in the literature.^[145-148] In 2018, Gabelli et al.^[149] demonstrated that the tunneling time in electrically driven metallic tunneling junction by quantum shot noise is as fast as 1 fs. The development and use of ultrashort pulsed lasers to excite electron tunneling across nanogaps has, since then, been shown to further set upper limits for the tunneling time of the order of attoseconds.^[3, 4, 6, 7] This, in principle, will enable optical-field-driven electron tunneling devices to operate at sub-optical-cycle timescale.^[150] The following section presents recent advances in optical-field-driven tunneling devices, focusing on the novel tunneling phenomenon based on different mechanisms.

4.1 Optical-field-driven direct tunneling devices

At present, the development of ultrafast optical-field-driven electron tunneling devices is still at the proof of principle stage. Though at a low technology readiness level, advances in materials science, coupled with access to novel fabrication processes and new excitation methodologies are helping to accelerate the technology development in this area towards an exciting opto-electronic integrated future. The present state-of-the-art is seeing researchers use ultrafast lasers to excite different asymmetric structures, allowing for the exploration of a range of exotic ultrafast electron emission processes in tunneling structures, some of which are explored here.

4.1.1 *Devices based on traditional materials*

Antenna coupled nanojunctions have attracted much attention due to their extremely high field-enhancement. Amongst the metallic nano-antenna structures, bow-ties have been widely used in high-harmonic generation,^[151, 152] optical rectification,^[150] attosecond electronics^[153, 154] and terahertz switching.^[155, 156] Similarly, bow-tie-related structures have been used in optical-field-driven electron tunneling devices to achieve high field-enhancement, briefly described in the following.

To combine the advantages of ultrafast femtosecond nano-optics with an on-chip communication scheme, optical signals with a frequency of several hundreds of THz need to be down-converted to coherent electronic signals capable of propagating on-chip. For this purpose, Holleitner et al.^[157] exploited femtosecond photo-switches based on asymmetric metallic nanogap junctions. They demonstrated that 14 fs optical pulses in the near-infrared can drive electronic circuits with a prospective bandwidth of up to 10 THz. More recently, the same

team demonstrated a unipolar ballistic electron current with an asymmetric metallic nanogap junction, which might be used for molecular electronics or as ultrafast photo-switches for THz electronics.^[158] **Figure 6a** shows the photoemission process of an asymmetric metal nanogap excited by an ultrafast laser pulse. As the laser field is plasmonically enhanced by the geometry's asymmetry, electrons are emitted from the emitter electrode into the gap and then to the collector electrode. The nonlinear photoemission processes associated with this transport are shown in **Figure 6b**. When the peak electric field amplitude of the laser, F_{laser} , is low ($\gamma \geq 1$), the emission current is dominated by multiphoton absorption (dashed red line in **Figure 6b**),^[60] and the power-law coefficient is similar to the number of absorbed photons.^[59] The electron emission can be described by the optical-field tunneling process (dashed green line in **Figure 6b**) when F_{laser} is high (> 10 V/nm).^[61]

Understanding the optical-field-driven electron dynamic in tunneling junctions has been found to be crucial in the design of integrated plasmonic and opto-electronic devices that operate at attosecond timescale. Brida et al.^[153] reported a coherent control of the electron tunneling control in a bow-tie structure using the CEP of a short-pulse laser. Due to the high field enhancement in the gap region (~ 35), the peak current densities of the device were very large (50 MA cm⁻²), and corresponded to the transfer of individual electrons in a half-cycle period of 2 fs. More recently, the same team measured interferometric autocorrelations of an ultrafast current induced by optical field emission across a nanogap consisting of a single plasmonic nanocircuit. It was shown that the measured response reflects the interplay between the CEP of the driving pulse, the plasmonic resonance of the antenna and quiver motion of the released electron.^[154] **Figure 6c** depicts the conceptual scheme of this experiment. The single-

cycle pulses were set to variable time delays Δt and then focused tightly onto a single plasmonic bow-tie antenna. The relative CEP of the biasing pulses could be fully controlled with a precision of 10 mrad. The Au nanoantenna features a 6 nm gap (inset of **Figure 6c**). Under a static time-invariant electric bias, this structure exhibits an I - V characteristic that is antisymmetric and highly nonlinear.^[153] As a result, an optically induced symmetry breaking occurs which leads to a net current that depends on the CEP of the driving pulse. Consequently, for a 2π CEP sweep, the integral current passes through a maximum, crosses zero and finally completely reverses its direction. The current measured as a function of the optical field amplitude of the single-cycle pulses is shown in **Figure 6d**. The current is modulated sinusoidally with a phase of φ that is directly related to the far-field CEP of the driving pulse $\varphi = \text{CEP} + \delta$. Understanding such optically driven electron dynamics at the nanoscale will facilitate control over electron transport on atomic time and length scales, which promises unprecedented precision and control for new devices, such as CEP photodetectors or ultrafast all-optical transistors and gates.

4.1.2 Devices based on low-dimensional nanomaterials

Nanocarbon materials have the potential to serve as an ideal material platform for the electron tunneling devices working in the optical-field-driven regime.^[72-74] Optical rectenna can directly convert free-propagating electromagnetic waves at optical frequencies to direct current.^[159] The cut-off frequency for a rectenna is defined as $f_c = 1/(2\pi R_A C_D)$,^[160] where R_A is the antenna resistance and C_D is the capacitance of the rectenna diode. The diode capacitance is given by $C_D = \epsilon_0 \epsilon A/d$, where ϵ_0 is the permittivity of vacuum, ϵ is the relative permittivity of the insulator, A is the area and d the insulator thickness. Diodes operating at cut-off frequencies on

the order of 1PHz (switching speed ~ 1 fs) are feasible if their capacitance is on the order of a few attofarads (aF).^[160, 161] This can be realized by a suitably designed antenna coupled to a diode. Cola et al.^[162] demonstrated an optical rectenna operating at 564 THz by engineering a MIM tunnel diode, with a junction capacitance of ~ 2 aF, at the tip of a vertically aligned multi-walled CNT (~ 10 nm in diameter), which acted as the antenna.^[163, 164] Due to self-assembly, nanocarbon-based devices are significantly easier to fabricate at the nanoscale than traditional materials-based devices, improving not only device yield but also the device optical cut-off frequency.

Recently, electronic control of an ultrafast tunneling electron emission source was demonstrated in a single-walled CNT(SWNT) nanogap irradiated by a femtosecond laser pulse,^[165] as schematically illustrated in **Figure 6e**. The photo-induced field emission in this SWNT device exhibited switching operation due to gate-induced variations in the effective barrier height. The photoelectron emission was tuned by gate-induced changes in the electronic band structures. As a result, the use of an SWNT provided an additional degree of freedom for controlling the electron emission yield and dynamic electron motion in the strong-field tunneling regime. Since then, nonlinear strong-field photoemission has recently been reported for a semiconducting SWNT emitter,^[165] which may prove particularly useful for future applications in attosecond electronics and photonics.

The atomically sharp edges and large crystallographic damage of the family of graphitic nanocarbons, and in particular graphene, are of key importance for their impressive ultrafast electron emission properties, specifically in the strong-field tunneling regime.^[166] As schematically illustrated in **Figure 6f**, strong photo-induced currents were produced when the

gap area was irradiated by a focused ultrashort pulse laser (wavelength, $\lambda = 800$ nm). Optical-field emission dominates the emission process for $\gamma \leq 1$, whereas γ has been limited to ~ 0.7 for $\lambda < 1$ μm . The graphene-based tunneling device achieved $\gamma < 0.5$ for an extremely low laser pulse energy of 15 pJ, owing to the large field enhancement of these 2D materials. At the maximum power condition, an extremely low Keldysh parameter of $\gamma = 0.2$ can be reached.^[166] For the low-power condition, most of the photo-emitted electrons undergo a quiver-motion and as a result, the electron wavepacket extends in time over an interval of the order of 10 fs. Conversely, in the high-power regime, more electrons are emitted in the sub-cycle, traversing the optical near-field of the antenna within less than one half cycle. This results in considerably shorter wavepackets than in the low-power case. A notable transition in the dynamic behavior of the electron emission can therefore be achieved by going from quiver motion to the sub-cycle motion with a change in the field intensity of the driving pulse. This result indicates that strong-field emission will allow for the creation of trains of ultrafast electron wavepackets with a temporal width of less than one half-cycle of the incident laser pulses. Ma et al.^[167] demonstrated the control of ultrafast electron thermalization in a graphene-hBN-graphene structure (**Figure 6g**), which showed a transition between different tunneling regimes and offered a means to modulate the electron energy transport in ultrafast tunneling dynamics. Some other low-dimensional nanomaterials, such as transition metal dichalcogenide (TMD), are also explored in optical-field-driven tunneling devices due to their optoelectronic properties.^[168] Sushko et al.^[169] reported large photocurrents upon optical excitation in h-BN/TMDs devices, which is attributed by Auger recombination in the TMDs. The primary difficulty in utilizing nanocarbon-based materials lies in their large-scale uniform preparation, however steady

progress continues to be made and such materials are viewed as being increasingly practical for deployment by many. In the near term, nanocarbon-based nanogaps will continue to be used to make important contributions to the development of tunable devices that can produce ultrashort electron pulses for future applications in table-top attosecond streaking, spatio-temporal imaging and high-speed electronics.

Most recently, using semiconducting CNT emitters, Dai et al.^[73] demonstrated an extreme nonlinear photoemission behavior in the strong-field regime.^[72, 170] In the case of 1D CNTs (**Figure 7a**), electron tunneling may start from conduction band (CB) states at a relatively low field due to the lower barrier height. However, the electron density in the edge of the valence band (VB) is much higher than that in the CB states. As a result, the emission current from the VB edge can be comparable to, or even larger than that from the CB (**Figure 7b**). **Figure 7c** shows the measured optical-field (F) dependent total photoemission current (I) for this CNT emitter. The I - F curve reveals a conventional strong-field photoemission behavior in the low-field section, with a transition the multiphoton photoemission (MPP) (gray pentagonal dots, **Figure 7c**) to an optical-field emission (OFE) regime (CB-OFE, green square, **Figure 7c**). At $F \approx 1.1 \text{ V nm}^{-1}$ (corresponding to $\gamma \approx 0.7$), an extremely nonlinear strong-field photoemission curve with a curve slope of up to 40 can be achieved and a new emission regime sets in which is termed the VB-OFE regime (purple circular, **Figure 7c**). As shown in **Figure 7d**, in the VB-OFE regime, I is modulated effectively with a depth up to 100% by changing the CEP. This result clearly shows that full access to the VB-OFE regime can offer more sensitive-CEP-control over the photoemission process than previously achieved. This is promising for the development of sensitive CEP detectors simply by using a source meter.^[3]

The high spatial and temporal resolution, high modulation sensitivity, control over the electron motion and sub-optical-cycle response of direct tunneling electronic devices ensure that such devices presents unprecedented potential in nonlinear optics, femtosecond and even attosecond opto-electronics.

4.2 Optical-field-driven resonant tunneling devices

Recently, the optical-field-driven method has been extended to other electron tunneling mechanisms, such as resonant tunneling^[171] and inelastic tunneling.^[172] Davidovich^[171] demonstrated a new model of time-dependent tunneling without the introduction of boundary conditions. Here they propose a joint solution of the time-dependent Schrödinger and Poisson equations, which is used to analyze the optical-field-driven double-barrier resonant tunneling diode. The model is based on an integral equation obtained by the time-dependent Green's function method. The potential function profile of a two-barrier structure is shown in **Figure 8a**, which depends on the doping profile and barrier widths. **Figure 8b** shows the calculated voltage U (1, right scale) and current density J (2, left scale) as a function of dimensionless time. A phase shift of approximately π is seen in Figure 8b, which indicates that the differential conductivity is negative and the structure can serve as a generator of ω_0 and $3\omega_0$ frequencies. This new model of time-dependent tunneling has been proposed to describe time-dependent resonant tunneling diodes and other structures with several barriers varying in time in a finite region, and can concurrently, be used to solve the open problem of the wavepacket tunneling time.^[173]

4.3 Optical-field-driven inelastic tunneling devices

Gordon et al.^[172] first demonstrated light-induced inelastic tunneling emission (LITE) in metal tunnel junctions. This device is shown schematically in **Figure 8c**. Similar to electric-field-driven inelastic tunneling device, it can produce photon emission. **Figure 8d** shows a schematic of this effect where the energy gap of a nanoscale self-assembled monolayer presents a tunneling barrier and the energy bias across the barrier oscillates with the applied field from the femtosecond pulse. **Figure 8e** shows the LITE spectra recorded on a fiber-coupled photon-counting spectrometer. The extremely bright emission from the LITE process can be observed by the naked eye. This phenomenon is promising for producing ultrafast upconverted light emission with higher efficiency than conventional nonlinear processes. By exploiting plasmonic resonances, the reduced tunneling bandwidth and more stable junction materials, LITE has significant potential for the realization of a highly efficient ultrafast source of upconverted photons.

Recent studies of optical-field-driven electron tunneling devices have already demonstrated great potential in achieving high working frequencies and in doing so have revealed a plethora of new and enticing physics in field-driven electron dynamics. Though moving rapidly, further theoretical and experimental research is crucially needed. For example, in the direct tunneling regime, transport in optical-field-driven electron dynamics in nanogap is not clear yet, in part due to the large parameter space which includes size and electronic structure of the nanoscale emitting tip, and the laser wavelength and intensity. Also, up to date, most of the work has focused on controlling electron dynamics optical-field emission in new types of tunneling devices. So far, only few studies have analyzed the interaction of the tunneling electrons with

solid-state quantum emitters. Such experiments are of crucial relevance for exploiting the enormous potential of tunneling devices in future ultrafast all-optical and quantum optical information processing.

5. Outlook

Primary studies have demonstrated that optically controlled electron tunneling through nanojunctions and nanogaps may, in principle, greatly increase the speed of future electronic devices by 5~6 orders of magnitude, providing unprecedented access to an entirely new class of electronics that are cable of operating at Peta-hertz (10^{15} Hz) frequencies. The atomic-scale tunneling emission surfaces of newly emerging low-dimensional materials, such as carbon nanomaterials, are proving to be key in the development of new approaches to sub-femtosecond duration tunneling; and in doing so will play a key role in achieving Peta-hertz devices. However, before achieving such a landmark achievement a number of major fundamental and technical challenges must be addressed. For instance, the fundamental physics of the process of optical-field-driven electron tunneling in low-dimensional nanoscale systems must be distinctive due to the quantized electronic structure, compared to traditional materials with continuous electronic structure. This should be further elucidated, with ongoing investigations into strongly coupled ultrafast dynamics such as electron-electron, electron-phonon, and electron-plasmon interactions, all of which are likely to require parameter decoupling through the use of extreme conditions including cryogenic temperatures and ultrashort laser pulses. Concurrent time-dependent ab-initio calculations will prove essential in the design of materials and device architectures. With a focus on materials, highly stable strong-field photoemission

materials, with unique properties such as low work function, high breakdown threshold, controllable and engineered doping profiles and band structures, designed by density functional theory and synthesized by atomic-precision additive-manufacturing will be an essential element of the emerging “lightwave electronics” toolbox. Most importantly, increasing studies of the interaction of tunneling electrons with quantum emitters are needed to devise new classes of all-optical and quantum optical switching devices. Such work offers the exciting prospect of merging some of the recent developments in ultrafast electron microscopy and tunneling devices, potentially providing a new level of control over the dynamics of electrons in functional nanodevices. With continued convergence of strong-field physics, attosecond technology, and materials science, optical-field-driven electron tunneling devices working at attosecond timescale are looking to be increasingly attainable. Based on optical-field-driven electron tunneling, such systems will drive a new paradigm in high-speed opto-electronics and in doing so will reshape modern information technology.

Acknowledgements

The authors acknowledge funding from the National Key R&D Program of China (Grant No. 2016YFA0202001), the National Natural Science Foundation of China (Grant No. 11427808, 51972072 and 51602071), the Key Research Program of the Chinese Academy of Sciences (grant no. ZDBS-SSW-JSC002), CAS Interdisciplinary Innovation Team (grant no. JCTD-2018-03), and the Strategic Priority Research Program of the Chinese Academy of Sciences (grant no. XDB50020200 and XDPB06).

Conflict of Interest

The authors declare no conflict of interest.

References

- [1] E. Goulielmakis, V. S. Yakovlev, A. L. Cavalieri, M. Uiberacker, V. Pervak, A. Apolonski, R. Kienberger, U. Kleineberg, F. Krausz, *Science* **2007**, 317, 769.
- [2] R. H. Dennard, F. H. Gaensslen, H. N. Yu, V. L. Rideout, E. Bassous, A. R. Leblanc, *Ieee Journal of Solid-State Circuits* **1974**, Sc 9, 256.
- [3] M. Kruger, M. Schenk, P. Hommelhoff, *Nature* **2011**, 475, 78.
- [4] G. Herink, D. R. Solli, M. Gulde, C. Ropers, *Nature* **2012**, 483, 190.
- [5] B. Piglosiewicz, S. Schmidt, D. J. Park, J. Vogelsang, P. Groß, C. Manzoni, P. Farinello, G. Cerullo, C. Lienau, *Nature Photonics* **2013**, 8, 37.
- [6] F. Krausz, M. Ivanov, *Reviews of Modern Physics* **2009**, 81, 163.
- [7] D. J. Park, B. Piglosiewicz, S. Schmidt, H. Kollmann, M. Mascheck, C. Lienau, *Phys Rev Lett* **2012**, 109, 244803.
- [8] S. Kumaragurubaran, T. Takahashi, Y. Masuda, S. Furuta, T. Sumiya, M. Ono, T. Shimizu, H. Suga, M. Horikawa, Y. Naitoh, *Applied Physics Letters* **2011**, 99, 263503.
- [9] W. H. Kim, C. S. Park, J. Y. Son, *Carbon* **2014**, 79, 388.
- [10] J. Yao, L. Zhong, Z. Zhang, T. He, Z. Jin, P. J. Wheeler, D. Natelson, J. M. Tour, *Small* **2009**, 5, 2910.
- [11] C. He, Z. Shi, L. Zhang, W. Yang, R. Yang, D. Shi, G. Zhang, *ACS Nano* **2012**, 6, 4214.
- [12] H. R. Park, X. S. Chen, N. C. Nguyen, J. Peraire, S. H. Oh, *Acs Photonics* **2015**, 2, 417.
- [13] L. N. Tripathi, Y. M. Bahk, G. Choi, S. Han, N. Park, D. S. Kim, *Applied Physics Express* **2016**, 9, 032001.
- [14] J. Keller, G. Scalari, S. Cibella, C. Maissen, F. Appugliese, E. Giovine, R. Leoni, M. Beck, J. Faist, *Nano Lett* **2017**, 17, 7410.
- [15] M. Kim, E. Pallecchi, R. J. Ge, X. H. Wu, G. Ducournau, J. C. Lee, H. Happy, D. Akinwande, *Nature Electronics* **2020**, 3, 479.
- [16] J. W. Han, D. I. Moon, M. Meyyappan, *Nano Lett* **2017**, 17, 2146.
- [17] A. Javey, J. Guo, Q. Wang, M. Lundstrom, H. Dai, *Nature* **2003**, 424, 654.
- [18] X. Du, I. Skachko, A. Barker, E. Y. Andrei, *Nat Nanotechnol* **2008**, 3, 491.
- [19] K. Boucart, A. M. Ionescu, *Ieee Transactions on Electron Devices* **2007**, 54, 1725.
- [20] F. Balestra, S. Cristoloveanu, M. Benachir, J. Brini, T. Elewa, *Ieee Electron Device Letters* **1987**, 8, 410.
- [21] S. Nirantar, T. Ahmed, G. Ren, P. Gutruf, C. Xu, M. Bhaskaran, S. Walia, S. Sriram, *Nano Lett* **2018**, 18, 7478.
- [22] J. W. Han, D. I. Moon, J. S. Oh, Y. K. Choi, M. Meyyappan, *Applied Physics Letters* **2014**, 104, 253506.
- [23] J. W. Han, M. L. Seol, D. I. Moon, G. Hunter, M. Meyyappan, *Nature Electronics* **2019**, 2, 405.
- [24] J.-W. Han, J. Sub Oh, M. Meyyappan, *Applied Physics Letters* **2012**, 100, 213505.
- [25] W. M. Jones, D. Lukin, A. Scherer, *Applied Physics Letters* **2017**, 110, 263101.
- [26] L. Pescini, A. Tilke, R. H. Blick, H. Lorenz, J. P. Kotthaus, W. Eberhardt, D. Kern, *Advanced Materials* **2001**, 13, 1780.
- [27] J. P. Sun, G. I. Haddad, P. Mazumder, J. N. Schulman, *Proceedings of the Ieee* **1998**, 86, 641.

- [28] M. Feiginov, C. Sydlo, O. Cojocari, P. Meissner, *Applied Physics Letters* **2011**, 99, 233506.
- [29] K. J. Gan, C. S. Tsai, Y. W. Chen, W. K. Yeh, *Solid-State Electronics* **2010**, 54, 1637.
- [30] N. Jin, S. Y. Chung, R. M. Heyns, P. R. Berger, R. H. Yu, P. E. Thompson, S. L. Rommel, *Ieee Electron Device Letters* **2004**, 25, 646.
- [31] Y. Koyama, R. Sekiguchi, T. Ouchi, *Applied Physics Express* **2013**, 6, 064102.
- [32] T. Maekawa, H. Kanaya, S. Suzuki, M. Asada, *Electronics Letters* **2014**, 50, 1214.
- [33] L. Esaki, *Physical Review* **1958**, 109, 603.
- [34] L. Esaki, R. Tsu, *Ibm Journal of Research and Development* **1970**, 14, 61.
- [35] Z. Shi, C. B. Simmons, J. R. Prance, J. K. Gamble, T. S. Koh, Y. P. Shim, X. Hu, D. E. Savage, M. G. Lagally, M. A. Eriksson, M. Friesen, S. N. Coppersmith, *Phys Rev Lett* **2012**, 108, 140503.
- [36] K. Y. Tan, K. W. Chan, M. Mottonen, A. Morello, C. Yang, J. van Donkelaar, A. Alves, J. M. Pirkkalainen, D. N. Jamieson, R. G. Clark, A. S. Dzurak, *Nano Lett* **2010**, 10, 11.
- [37] J. Verduijn, G. C. Tettamanzi, S. Rogge, *Nano Lett* **2013**, 13, 1476.
- [38] D. Culcer, A. L. Saraiva, B. Koiller, X. Hu, S. Das Sarma, *Phys Rev Lett* **2012**, 108, 126804.
- [39] M. Amman, R. Wilkins, E. Ben-Jacob, P. D. Maker, R. C. Jaklevic, *Phys Rev B Condens Matter* **1991**, 43, 1146.
- [40] A. E. Hanna, M. Tinkham, *Phys Rev B Condens Matter* **1991**, 44, 5919.
- [41] M. Parzefall, P. Bharadwaj, A. Jain, T. Taniguchi, K. Watanabe, L. Novotny, *Nat Nanotechnol* **2015**, 10, 1058.
- [42] H. L. Qian, S. W. Hsu, K. Gurunatha, C. T. Riley, J. Zhao, D. Lu, A. R. Tao, Z. W. Liu, *Nature Photonics* **2018**, 12, 485.
- [43] J. Kern, R. Kulloock, J. Prangma, M. Emmerling, M. Kamp, B. Hecht, *Nature Photonics* **2015**, 9, 582.
- [44] W. Du, T. Wang, H.-S. Chu, C. A. Nijhuis, *Nature Photonics* **2017**, 11, 623.
- [45] P. Wang, A. V. Krasavin, M. E. Nasir, W. Dickson, A. V. Zayats, *Nat Nanotechnol* **2018**, 13, 159.
- [46] H. Chalabi, D. Schoen, M. L. Brongersma, *Nano Lett* **2014**, 14, 1374.
- [47] J. A. Misewich, R. Martel, P. Avouris, J. C. Tsang, S. Heinze, J. Tersoff, *Science* **2003**, 300, 783.
- [48] P. Rai, N. Hartmann, J. Berthelot, J. Arocas, G. Colas des Francs, A. Hartschuh, A. Bouhelier, *Phys Rev Lett* **2013**, 111, 026804.
- [49] S. Namgung, D. A. Mohr, D. Yoo, P. Bharadwaj, S. J. Koester, S. H. Oh, *ACS Nano* **2018**, 12, 2780.
- [50] M. Parzefall, A. Szabo, T. Taniguchi, K. Watanabe, M. Luisier, L. Novotny, *Nat Commun* **2019**, 10, 292.
- [51] R. Berndt, J. K. Gimzewski, P. Johansson, *Phys Rev Lett* **1991**, 67, 3796.
- [52] N. J. Halas, S. Lal, W. S. Chang, S. Link, P. Nordlander, *Chem Rev* **2011**, 111, 3913.
- [53] C. Ciraci, R. T. Hill, J. J. Mock, Y. Urzhumov, A. I. Fernandez-Dominguez, S. A. Maier, J. B. Pendry, A. Chilkoti, D. R. Smith, *Science* **2012**, 337, 1072.
- [54] Z. J. Li, B. Bai, C. Li, Q. Dai, *Carbon* **2016**, 96, 641.
- [55] C. Li, Z. Li, C. Ke, B. Bing, D. Qing, *Applied Physics Letters* **2017**, 110, 093105.

- [56] M. Vahdani Moghaddam, P. Yaghoobi, G. A. Sawatzky, A. Nojeh, *ACS Nano* **2015**, 9, 4064.
- [57] L. Seiffert, T. Paschen, P. Hommelhoff, T. Fennel, *Journal of Physics B-Atomic Molecular and Optical Physics* **2018**, 51, 134001.
- [58] P. Hommelhoff, C. Kealhofer, M. A. Kasevich, *Phys Rev Lett* **2006**, 97, 247402.
- [59] L. V. Keldysh, *Soviet Physics Jetp-Ussr* **1965**, 20, 1307.
- [60] P. Musumeci, L. Cultrera, M. Ferrario, D. Filippetto, G. Gatti, M. S. Gutierrez, J. T. Moody, N. Moore, J. B. Rosenzweig, C. M. Scoby, G. Travish, C. Vicario, *Phys Rev Lett* **2010**, 104, 084801.
- [61] M. F. Ciappina, J. A. Perez-Hernandez, A. S. Landsman, W. A. Okell, S. Zherebtsov, B. Forg, J. Schotz, L. Seiffert, T. Fennel, T. Shaaran, T. Zimmermann, A. Chacon, R. Guichard, A. Zair, J. W. Tisch, J. P. Marangos, T. Witting, A. Braun, S. A. Maier, L. Roso, M. Kruger, P. Hommelhoff, M. F. Kling, F. Krausz, M. Lewenstein, *Rep. Prog. Phys.* **2017**, 80, 054401.
- [62] P. Dombi, Z. Pápa, J. Vogelsang, S. V. Yalunin, M. Siviš, G. Herink, S. Schäfer, P. Groß, C. Ropers, C. Lienau, *Reviews of Modern Physics* **2020**, 92, 66.
- [63] Y. C. Chen, S. Z. Deng, N. S. Xu, J. Chen, *Applied Physics Letters* **2020**, 116.
- [64] V. Dubois, S. J. Bleiker, G. Stemme, F. Niklaus, *Adv Mater* **2018**, 30, e1801124.
- [65] K. J. Kaltenecker, E. Krauss, L. Casses, M. Geisler, B. Hecht, N. A. Mortensen, P. U. Jepsen, N. Stenger, *Nanophotonics* **2020**, 9, 509.
- [66] J. S. Huang, V. Callegari, P. Geisler, C. Bruning, J. Kern, J. C. Prangsma, X. Wu, T. Feichtner, J. Ziegler, P. Weinmann, M. Kamp, A. Forchel, P. Biagioni, U. Sennhauser, B. Hecht, *Nat Commun* **2010**, 1, 150.
- [67] A. V. Eletsii, *Physics-Uspokhi* **2010**, 53, 863.
- [68] W. Zhu, C. Bower, O. Zhou, G. Kochanski, S. Jin, *Applied Physics Letters* **1999**, 75, 873.
- [69] T. Kim, J. S. Lee, K. Li, T. J. Kang, Y. H. Kim, *Carbon* **2016**, 101, 345.
- [70] N. O. Weiss, H. Zhou, L. Liao, Y. Liu, S. Jiang, Y. Huang, X. Duan, *Adv Mater* **2012**, 24, 5782.
- [71] Y. C. Chen, L. W. Liu, K. S. Zheng, J. C. She, S. Z. Deng, N. S. Xu, J. Chen, *Advanced Electronic Materials* **2019**, 5.
- [72] C. Li, X. Zhou, F. Zhai, Z. Li, F. Yao, R. Qiao, K. Chen, M. T. Cole, D. Yu, Z. Sun, K. Liu, Q. Dai, *Adv Mater* **2017**, 29, 1701580.
- [73] C. Li, K. Chen, M. Guan, X. Wang, X. Zhou, F. Zhai, J. Dai, Z. Li, Z. Sun, S. Meng, K. Liu, Q. Dai, *Nat Commun* **2019**, 10, 4891.
- [74] S. Zhou, K. Chen, M. T. Cole, Z. Li, J. Chen, C. Li, Q. Dai, *Adv Mater* **2019**, 31, e1805845.
- [75] C. Li, Y. Zhang, M. Mann, P. Hiralal, H. E. Unalan, W. Lei, B. P. Wang, D. P. Chu, D. Pribat, G. A. J. Amaratunga, W. I. Milne, *Applied Physics Letters* **2010**, 96, 143114.
- [76] C. Li, Y. Zhang, M. T. Cole, S. G. Shivareddy, J. S. Barnard, W. Lei, B. Wang, D. Pribat, G. A. Amaratunga, W. I. Milne, *ACS Nano* **2012**, 6, 3236.
- [77] K. Otsuka, T. Inoue, Y. Shimomura, S. Chiashi, S. Maruyama, *Nanoscale* **2016**, 8, 16363.
- [78] R. H. Fowler, L. Nordheim, *Proceedings of the Royal Society of London Series a-Containing Papers of a Mathematical and Physical Character* **1928**, 119, 173.
- [79] E. L. Murphy, R. H. Good, *Physical Review* **1956**, 102, 1464.
- [80] J. Xu, Z. Gu, W. Yang, Q. Wang, X. Zhang, *Nanoscale Res Lett* **2018**, 13, 311.

- [81] H. M. Wang, Z. Zheng, Y. Y. Wang, J. J. Qiu, Z. B. Guo, Z. X. Shen, T. Yu, *Applied Physics Letters* **2010**, 96, 023106.
- [82] S. Kumar, G. S. Duesberg, R. Pratap, S. Raghavan, *Applied Physics Letters* **2014**, 105, 103107.
- [83] V. L. Katkov, V. A. Osipov, *Applied Physics Letters* **2014**, 104, 053102.
- [84] X. Wang, Y. Ouyang, X. Li, H. Wang, J. Guo, H. Dai, *Phys Rev Lett* **2008**, 100, 206803.
- [85] S. Srisonphan, M. Kim, H. K. Kim, *Sci Rep* **2014**, 4, 3764.
- [86] G. T. Wu, X. L. Wei, Z. Y. Zhang, Q. Chen, L. M. Peng, *Advanced Functional Materials* **2015**, 25, 5972.
- [87] C. Zeng, E. B. Song, M. Wang, S. Lee, C. M. Torres, Jr., J. Tang, B. H. Weiller, K. L. Wang, *Nano Lett* **2013**, 13, 2370.
- [88] S. Vaziri, G. Lupina, C. Henkel, A. D. Smith, M. Ostling, J. Dabrowski, G. Lippert, W. Mehr, M. C. Lemme, *Nano Lett* **2013**, 13, 1435.
- [89] W. Mehr, J. Dabrowski, J. C. Scheytt, G. Lippert, Y. H. Xie, M. C. Lemme, M. Ostling, G. Lupina, *Ieee Electron Device Letters* **2012**, 33, 691.
- [90] T. Georgiou, R. Jalil, B. D. Belle, L. Britnell, R. V. Gorbachev, S. V. Morozov, Y. J. Kim, A. Gholinia, S. J. Haigh, O. Makarovskiy, L. Eaves, L. A. Ponomarenko, A. K. Geim, K. S. Novoselov, A. Mishchenko, *Nat Nanotechnol* **2013**, 8, 100.
- [91] Y. Chen, Z. Li, J. Chen, *ACS Appl Mater Interfaces* **2020**, 12, 57505.
- [92] P. See, D. J. Paul, B. Hollander, S. Mantl, I. V. Zozoulenko, K. F. Berggren, *Ieee Electron Device Letters* **2001**, 22, 182.
- [93] P. See, D. J. Paul, *Ieee Electron Device Letters* **2001**, 22, 582.
- [94] Y. X. Liao, P. F. Zhang, S. Bremner, S. Shrestha, S. J. Huang, G. Conibeer, *Advanced Functional Materials* **2017**, 27, 1605348.
- [95] T. P. E. Broekaert, W. Lee, C. G. Fonstad, *Applied Physics Letters* **1988**, 53, 1545.
- [96] L. F. Luo, R. Beresford, W. I. Wang, *Applied Physics Letters* **1989**, 55, 2023.
- [97] A. Pfenning, F. Hartmann, R. Weih, M. Emmerling, L. Worschech, S. Hofling, *Advanced Optical Materials* **2018**, 6, 1800972.
- [98] B. Tao, C. Wan, P. Tang, J. Feng, H. Wei, X. Wang, S. Andrieu, H. Yang, M. Chshiev, X. Devaux, T. Hauet, F. Montaigne, S. Mangin, M. Hehn, D. Lacour, X. Han, Y. Lu, *Nano Lett* **2019**, 19, 3019.
- [99] Q. Xiang, H. Sukegawa, M. Belmoubarik, M. Al-Mahdawi, T. Scheike, S. Kasai, Y. Miura, S. Mitani, *Adv Sci (Weinh)* **2019**, 6, 1901438.
- [100] S. Lee, Y. Lee, E. B. Song, T. Hiramoto, *Journal of Applied Physics* **2013**, 114, 164513.
- [101] S. Lee, Y. Lee, E. B. Song, T. Hiramoto, *Nano Lett* **2014**, 14, 71.
- [102] G. Yang, L. Tan, Y. Yang, S. Chen, G.-Y. Liu, *Surface Science* **2005**, 589, 129.
- [103] R. Negishi, T. Hasegawa, K. Terabe, M. Aono, H. Tanaka, T. Ogawa, H. Ozawa, *Applied Physics Letters* **2007**, 90, 223112.
- [104] R. Hayakawa, N. Hiroshiba, T. Chikyow, Y. Wakayama, *Advanced Functional Materials* **2011**, 21, 2933.
- [105] Q. Schaefferbeke, R. Avriker, T. Frederiksen, F. Pistolesi, *Phys Rev Lett* **2019**, 123, 246601.
- [106] Y. Jing, S. Huang, J. Wu, M. Meng, X. Li, Y. Zhou, H. Peng, H. Xu, *Adv Mater* **2019**, 31, e1903686.

- [107] D. L. Klein, R. Roth, A. K. L. Lim, A. P. Alivisatos, P. L. McEuen, *Nature* **1997**, 389, 699.
- [108] T. Wagner, P. Talkner, J. C. Bayer, E. P. Rugeramigabo, P. Hanggi, R. J. Haug, *Nature Physics* **2019**, 15, 330.
- [109] C. Gong, H. J. Zhang, W. H. Wang, L. Colombo, R. M. Wallace, K. J. Cho, *Applied Physics Letters* **2013**, 103, 053513.
- [110] J. Shewchun, V. A. K. Temple, *Journal of Applied Physics* **1972**, 43, 5051.
- [111] M. Chhowalla, D. Jena, H. Zhang, *Nature Reviews Materials* **2016**, 1, 1.
- [112] A. K. Geim, I. V. Grigorieva, *Nature* **2013**, 499, 419.
- [113] M. Huang, S. Li, Z. Zhang, X. Xiong, X. Li, Y. Wu, *Nat Nanotechnol* **2017**, 12, 1148.
- [114] X. H. Mou, L. F. Register, A. H. MacDonald, S. K. Banerjee, *Ieee Transactions on Electron Devices* **2017**, 64, 4759.
- [115] R. Yan, G. Khalsa, S. Vishwanath, Y. Han, J. Wright, S. Rouvimov, D. S. Katzer, N. Nepal, B. P. Downey, D. A. Muller, H. G. Xing, D. J. Meyer, D. Jena, *Nature* **2018**, 555, 183.
- [116] K. S. Novoselov, D. Jiang, F. Schedin, T. J. Booth, V. V. Khotkevich, S. V. Morozov, A. K. Geim, *Proc Natl Acad Sci U S A* **2005**, 102, 10451.
- [117] C. X. Zhang, C. Gong, Y. F. Nie, K. A. Min, C. P. Liang, Y. J. Oh, H. J. Zhang, W. H. Wang, S. Hong, L. Colombo, R. M. Wallace, K. Cho, *2d Materials* **2017**, 4, 015026.
- [118] Y. C. Lin, R. K. Ghosh, R. Addou, N. Lu, S. M. Eichfeld, H. Zhu, M. Y. Li, X. Peng, M. J. Kim, L. J. Li, R. M. Wallace, S. Datta, J. A. Robinson, *Nat Commun* **2015**, 6, 7311.
- [119] L. Britnell, R. V. Gorbachev, R. Jalil, B. D. Belle, F. Schedin, M. I. Katsnelson, L. Eaves, S. V. Morozov, A. S. Mayorov, N. M. Peres, A. H. Neto, J. Leist, A. K. Geim, L. A. Ponomarenko, K. S. Novoselov, *Nano Lett* **2012**, 12, 1707.
- [120] G. H. Lee, Y. J. Yu, C. Lee, C. Dean, K. L. Shepard, P. Kim, J. Hone, *Applied Physics Letters* **2011**, 99, 243114.
- [121] L. Britnell, R. V. Gorbachev, A. K. Geim, L. A. Ponomarenko, A. Mishchenko, M. T. Greenaway, T. M. Fromhold, K. S. Novoselov, L. Eaves, *Nat Commun* **2013**, 4, 1794.
- [122] A. Mishchenko, J. S. Tu, Y. Cao, R. V. Gorbachev, J. R. Wallbank, M. T. Greenaway, V. E. Morozov, S. V. Morozov, M. J. Zhu, S. L. Wong, F. Withers, C. R. Woods, Y. J. Kim, K. Watanabe, T. Taniguchi, E. E. Vdovin, O. Makarovskiy, T. M. Fromhold, V. I. Fal'ko, A. K. Geim, L. Eaves, K. S. Novoselov, *Nat Nanotechnol* **2014**, 9, 808.
- [123] C. R. Dean, A. F. Young, I. Meric, C. Lee, L. Wang, S. Sorgenfrei, K. Watanabe, T. Taniguchi, P. Kim, K. L. Shepard, J. Hone, *Nat Nanotechnol* **2010**, 5, 722.
- [124] C. R. Woods, L. Britnell, A. Eckmann, R. S. Ma, J. C. Lu, H. M. Guo, X. Lin, G. L. Yu, Y. Cao, R. V. Gorbachev, A. V. Kretinin, J. Park, L. A. Ponomarenko, M. I. Katsnelson, Y. N. Gornostyrev, K. Watanabe, T. Taniguchi, C. Casiraghi, H. J. Gao, A. K. Geim, K. S. Novoselov, *Nature Physics* **2014**, 10, 451.
- [125] J. Xue, J. Sanchez-Yamagishi, D. Bulmash, P. Jacquod, A. Deshpande, K. Watanabe, T. Taniguchi, P. Jarillo-Herrero, B. J. LeRoy, *Nat Mater* **2011**, 10, 282.
- [126] M. Yankowitz, J. Xue, D. Cormode, J. D. Sanchez-Yamagishi, K. Watanabe, T. Taniguchi, P. Jarillo-Herrero, P. Jacquod, B. J. LeRoy, *Nature Physics* **2012**, 8, 382.
- [127] C. R. Dean, L. Wang, P. Maher, C. Forsythe, F. Ghahari, Y. Gao, J. Katoch, M. Ishigami, P. Moon, M. Koshino, T. Taniguchi, K. Watanabe, K. L. Shepard, J. Hone, P. Kim, *Nature* **2013**, 497, 598.
- [128] B. Hunt, J. D. Sanchez-Yamagishi, A. F. Young, M. Yankowitz, B. J. LeRoy, K. Watanabe,

- T. Taniguchi, P. Moon, M. Koshino, P. Jarillo-Herrero, R. C. Ashoori, *Science* **2013**, 340, 1427.
- [129] L. A. Ponomarenko, R. V. Gorbachev, G. L. Yu, D. C. Elias, R. Jalil, A. A. Patel, A. Mishchenko, A. S. Mayorov, C. R. Woods, J. R. Wallbank, M. Mucha-Kruczynski, B. A. Piot, M. Potemski, I. V. Grigorieva, K. S. Novoselov, F. Guinea, V. I. Fal'ko, A. K. Geim, *Nature* **2013**, 497, 594.
- [130] G. Kim, S. S. Kim, J. Jeon, S. I. Yoon, S. Hong, Y. J. Cho, A. Misra, S. Ozdemir, J. Yin, D. Ghazaryan, M. Holwill, A. Mishchenko, D. V. Andreeva, Y. J. Kim, H. Y. Jeong, A. R. Jang, H. J. Chung, A. K. Geim, K. S. Novoselov, B. H. Sohn, H. S. Shin, *Nat Commun* **2019**, 10, 230.
- [131] X. Xiong, M. Q. Huang, B. Hu, X. F. Li, F. Liu, S. C. Li, M. C. Tian, T. Y. Li, J. Song, Y. Q. Wu, *Nature Electronics* **2020**, 3, 106.
- [132] A. Yangui, M. Bescond, T. Yan, N. Nagai, K. Hirakawa, *Nat Commun* **2019**, 10, 4504.
- [133] S. Zheng, S. Jo, K. Kang, L. Sun, M. Zhao, K. Watanabe, T. Taniguchi, P. Moon, N. Myoung, H. Yang, *Adv Mater* **2020**, 32, e1906942.
- [134] J. Lambe, S. L. McCarthy, *Physical Review Letters* **1976**, 37, 923.
- [135] P. Johansson, R. Monreal, P. Apell, *Phys Rev B Condens Matter* **1990**, 42, 9210.
- [136] P. Bharadwaj, A. Bouhelier, L. Novotny, *Phys Rev Lett* **2011**, 106, 226802.
- [137] A. Nevet, N. Berkovitch, A. Hayat, P. Ginzburg, S. Ginzach, O. Sorias, M. Orenstein, *Nano Lett* **2010**, 10, 1848.
- [138] A. G. Curto, T. H. Taminiau, G. Volpe, M. P. Kreuzer, R. Quidant, N. F. van Hulst, *Nat Commun* **2013**, 4, 1750.
- [139] J. C. Prangma, J. Kern, A. G. Knapp, S. Grossmann, M. Emmerling, M. Kamp, B. Hecht, *Nano Lett* **2012**, 12, 3915.
- [140] B. Huang, S. Gao, Y. Liu, J. Wang, Z. Liu, Y. Guo, W. Lu, *Opt Lett* **2019**, 44, 2330.
- [141] M. Doderer, M. Parzefall, A. Joerg, D. Chelladurai, N. Dordevic, Y. Fedoryshyn, A. Agrawal, H. J. Lezec, L. Novotny, J. Leuthold, C. Haffner, Ieee, in *2019 Conference on Lasers and Electro-Optics*, **2019**.
- [142] A. K. Geim, K. S. Novoselov, *Nat Mater* **2007**, 6, 183.
- [143] R. R. Nair, P. Blake, A. N. Grigorenko, K. S. Novoselov, T. J. Booth, T. Stauber, N. M. Peres, A. K. Geim, *Science* **2008**, 320, 1308.
- [144] K. F. Mak, M. Y. Sfeir, Y. Wu, C. H. Lui, J. A. Misewich, T. F. Heinz, *Phys Rev Lett* **2008**, 101, 196405.
- [145] L. Wu, H. Duan, P. Bai, M. Bosman, J. K. Yang, E. Li, *ACS Nano* **2013**, 7, 707.
- [146] M. Uiberacker, T. Uphues, M. Schultze, A. J. Verhoef, V. Yakovlev, M. F. Kling, J. Rauschenberger, N. M. Kabachnik, H. Schroder, M. Lezius, K. L. Kompa, H. G. Muller, M. J. Vrakking, S. Hendel, U. Kleineberg, U. Heinzmann, M. Drescher, F. Krausz, *Nature* **2007**, 446, 627.
- [147] G. Nimtz, *Foundations of Physics* **2011**, 41, 1193.
- [148] K. K. Thornber, T. C. McGill, C. A. Mead, *Journal of Applied Physics* **1967**, 38, 2384.
- [149] P. Fevrier, J. Gabelli, *Nat Commun* **2018**, 9, 4940.
- [150] D. R. Ward, F. Huser, F. Pauly, J. C. Cuevas, D. Natelson, *Nat Nanotechnol* **2010**, 5, 732.
- [151] S. Kim, J. Jin, Y. J. Kim, I. Y. Park, Y. Kim, S. W. Kim, *Nature* **2008**, 453, 757.
- [152] M. Sivilis, M. Duwe, B. Abel, C. Ropers, *Nature Physics* **2013**, 9, 304.

- [153] T. Rybka, M. Ludwig, M. F. Schmalz, V. Knittel, D. Brida, A. Leitenstorfer, *Nature Photonics* **2016**, 10, 667.
- [154] M. Ludwig, G. Aguirregabiria, F. Ritzkowski, T. Rybka, D. C. Marinica, J. Aizpurua, A. G. Borisov, A. Leitenstorfer, D. Brida, *Nature Physics* **2019**, 16, 341.
- [155] P. Lang, B. Ji, X. Song, Y. Dou, H. Tao, X. Gao, Z. Hao, J. Lin, *Opt Lett* **2018**, 43, 5721.
- [156] M. Samizadeh Nikoo, A. Jafari, N. Perera, M. Zhu, G. Santoruvo, E. Matioli, *Nature* **2020**, 579, 534.
- [157] C. Karnetzky, P. Zimmermann, C. Trummer, C. Duque Sierra, M. Worle, R. Kienberger, A. Holleitner, *Nat Commun* **2018**, 9, 2471.
- [158] P. Zimmermann, A. Hotger, N. Fernandez, A. Nolinder, K. Muller, J. J. Finley, A. W. Holleitner, *Nano Lett* **2019**, 19, 1172.
- [159] R. L. Bailey, *Journal of Engineering for Power* **1972**, 94, 73.
- [160] A. Sanchez, C. F. Davis, K. C. Liu, A. Javan, *Journal of Applied Physics* **1978**, 49, 5270.
- [161] G. Moddel, S. Grover, *Rectenna Solar Cells*, Springer, **2013**.
- [162] A. Sharma, V. Singh, T. L. Bougher, B. A. Cola, *Nat Nanotechnol* **2015**, 10, 1027.
- [163] Y. Wang, K. Kempa, B. Kimball, J. B. Carlson, G. Benham, W. Z. Li, T. Kempa, J. Rybczynski, A. Herczynski, Z. F. Ren, *Applied Physics Letters* **2004**, 85, 2607.
- [164] K. Kempa, J. Rybczynski, Z. P. Huang, K. Gregorczyk, A. Vidan, B. Kimball, J. Carlson, G. Benham, Y. Wang, A. Herczynski, Z. F. Ren, *Advanced Materials* **2007**, 19, 421.
- [165] B. H. Son, D. J. Park, Y. H. Ahn, *Applied Physics Letters* **2019**, 115, 163102.
- [166] B. H. Son, H. S. Kim, J. Y. Park, S. Lee, D. J. Park, Y. H. Ahn, *Acs Photonics* **2018**, 5, 3943.
- [167] Q. Ma, T. I. Andersen, N. L. Nair, N. M. Gabor, M. Massicotte, C. H. Lui, A. F. Young, W. J. Fang, K. Watanabe, T. Taniguchi, J. Kong, N. Gedik, F. H. L. Koppens, P. Jarillo-Herrero, *Nature Physics* **2016**, 12, 455.
- [168] K. F. Mak, J. Shan, *Nature Photonics* **2016**, 10, 216.
- [169] A. Sushko, K. De Greve, M. Phillips, B. Urbaszek, A. Y. Joe, K. Watanabe, T. Taniguchi, A. L. Efros, C. S. Hellberg, H. Park, P. Kim, M. D. Lukin, *Nanophotonics* **2020**, 10, 105.
- [170] C. Li, X. Zhou, F. Zhai, Z. J. Li, F. R. Yao, R. X. Qiao, K. Chen, D. P. Yu, Z. P. Sun, K. H. Liu, Q. Dai, *Applied Physics Letters* **2017**, 111, 133101.
- [171] M. V. Davidovich, *Jetp Letters* **2019**, 110, 472.
- [172] E. Rakhmatov, A. Alizadehkhaledi, G. Hajisalem, R. Gordon, *Opt Express* **2020**, 28, 16497.
- [173] A. B. Shvartsburg, *Physics-Uspekhi* **2007**, 50, 37.

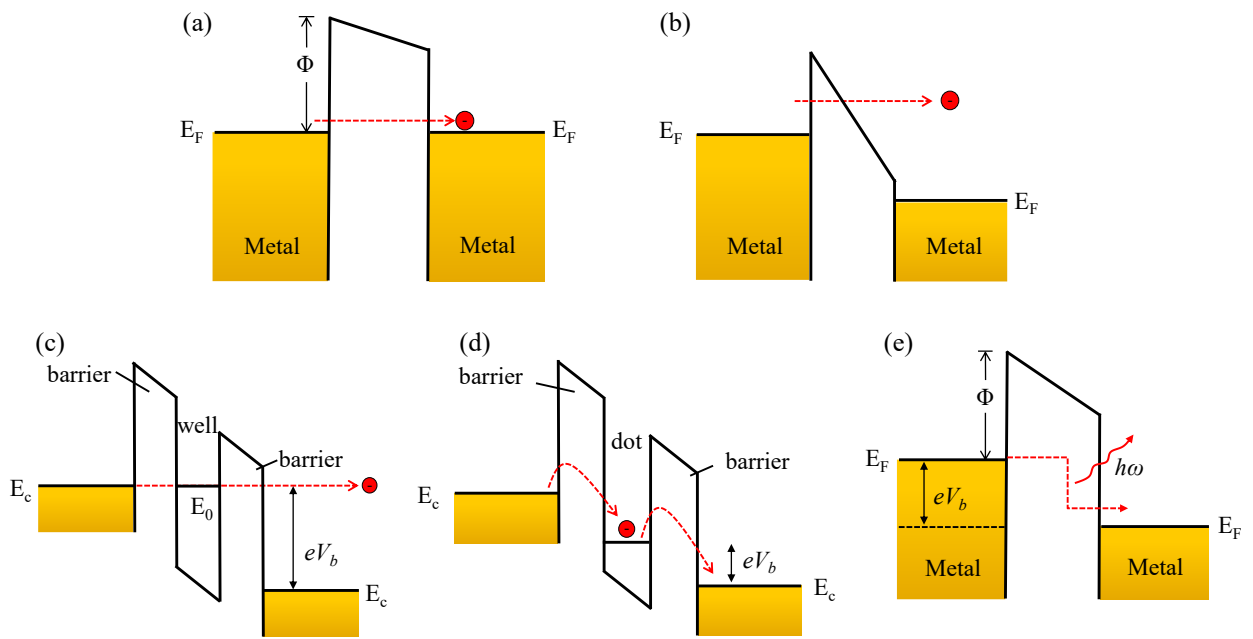


Figure 1. The principles of electric-field-driven tunneling. (a) Energy band diagram for direct tunneling. E_f , Fermi level; Φ , barrier height; V_G , gate voltage. (b) Energy band diagram for F-N tunneling. (c) Energy band diagram for resonant tunneling. E_c , Fermi level of the electrode; E_0 , Fermi level of the potential well; V_b , applied bias. (d) Energy band diagram of single-electron tunneling devices. The electron can only tunnel through the barrier one by one due to Coulomb blockade effects. (e) Energy band diagram for inelastic tunneling. $\hbar\omega$, photon energy.

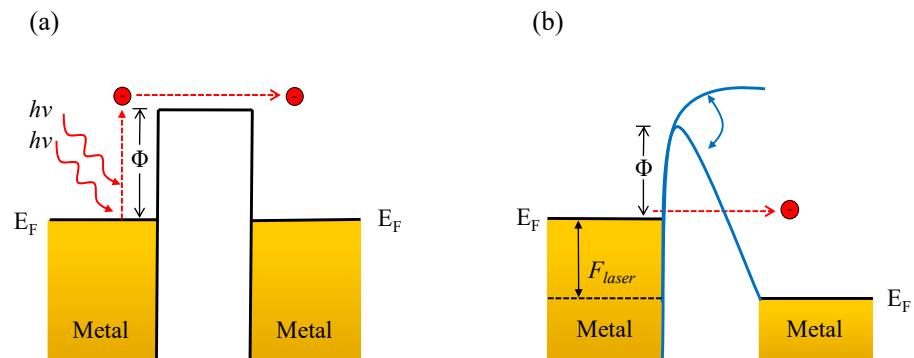


Figure 2. Mechanisms of optical-field-driven tunneling. (a) Multiphoton emission. An electron absorbs the energy of a number of photons to overcome the barrier for photoemission. E_F , Fermi level; Φ , barrier height. (b) Optical-field tunneling emission. A strong optical field induces a periodically oscillating barrier at an optical-frequency of ω . When the optical field is strong enough to create a penetrable tunneling barrier, electrons tunnel from the Fermi level in a fraction of a negative half optical-cycle.

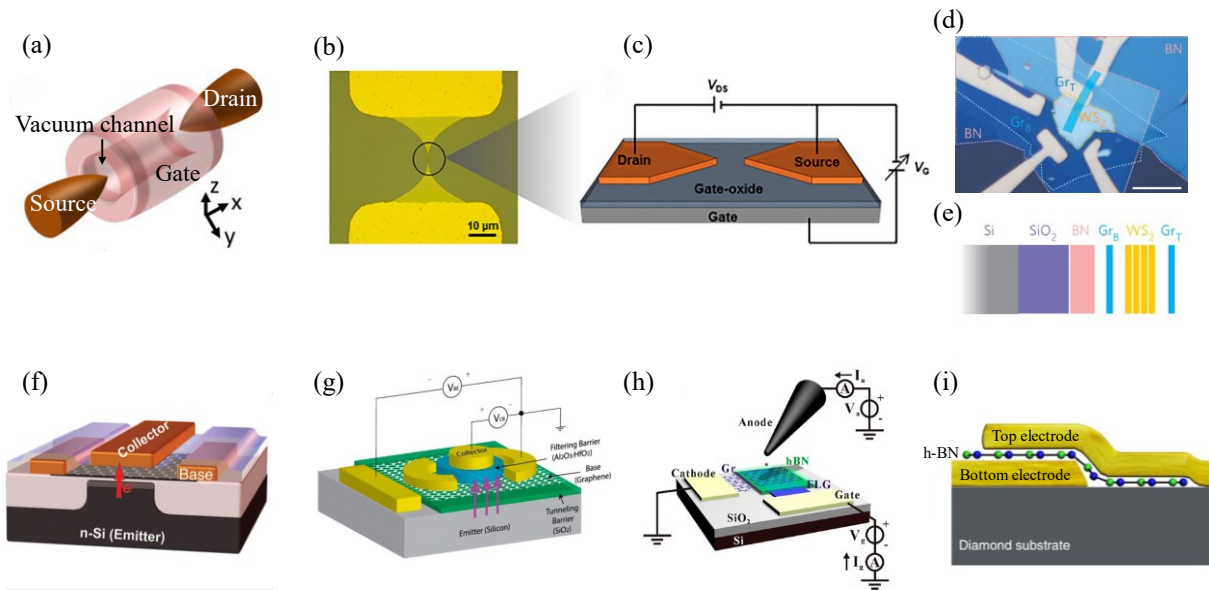


Figure 3. Representative direct tunneling devices. (a) Schematic illustrations of a surround-gate electron tunneling device. Reproduced with permission. Copyright 2017,^[16] American Chemical Society. (b-c) Metal-air-metal tunneling device consist of two in-plan symmetric metal electrodes. (b) Top view optical image of fabricated device. (c) Schematic illustration of the device structure with a biasing scheme. The metal-air-metal structure depicts drain and source configuration. A dielectric thin film offers separation from conductive back-gate. (b-c) Reproduced with permission.^[21] Copyright 2018, American Chemical Society. (d) Optical image and (e) vertical architecture of graphene-WS₂tunneling transistor. (d-e) Reproduced with permission.^[90] Copyright 2013, Nature Publishing Group. (f) Schematic structure of the graphene-based hot electron tunneling transistor. During device operation, hot carriers are injected from the emitter across the emitter-base insulator and the graphene base into the collector, as indicated by the red arrow. Reproduced with permission.^[88] Copyright 2013, American Chemical Society. (g) Schematic diagram of the graphene-based hot electron tunneling transistor and the common-base configuration used to measure the I–V characteristics. Graphene is used as the base region for a hot electron transistor structure. The purple arrows indicate the transport direction of the hot electrons. Reproduced with permission.^[87] Copyright 2013, American Chemical Society. (h) The schematic diagram of the graphene/h-BN hot carrier tunneling device. An anode probe with a voltage of V_a is placed at a distance d above the device. The gate is in a bias of V_g and the cathode is grounded. The anode current I_a and gate current I_g are recorded simultaneously. Reproduced with permission.^[91] Copyright 2020, American Chemical Society. (i) Simplified side-view illustration of the monolayer h-BN radio-frequency switch based on metal-insulator-metal (MIM) tunneling device. Reproduced with permission.^[15] Copyright 2020, Nature Publishing Group.

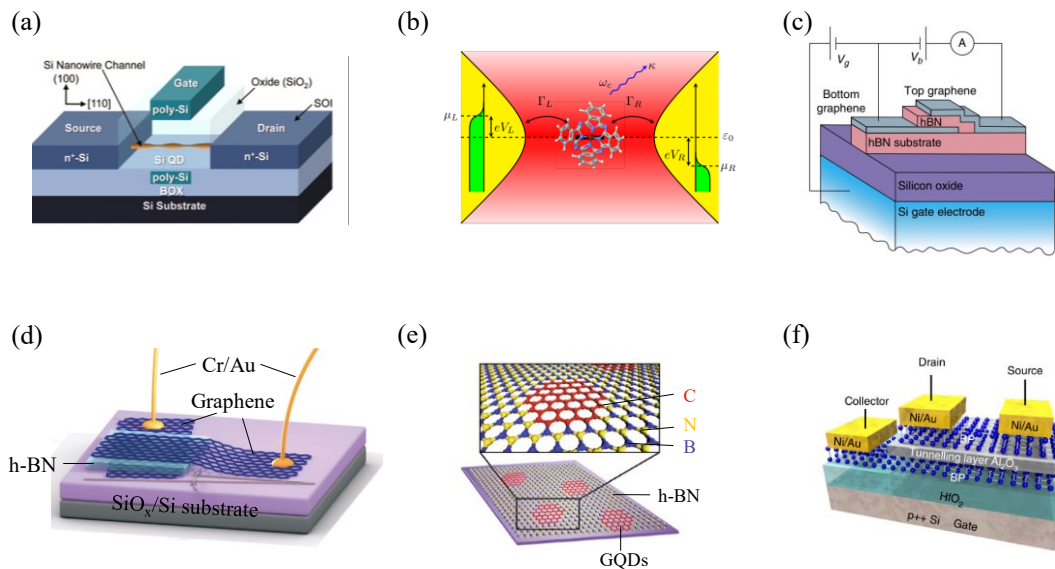


Figure 4. Representative resonant tunneling devices. (a) Schematic configuration of the Si-quantum-dot-based single-electron transistor (SET). Reproduced with permission.^[101] Copyright 2014, American Chemical Society. (b) Schematic of a typical molecule-based SET. Two metallic electrodes forming a plasmonic nanocavity characterized by a resonance frequency $\omega_c/2\pi$ and damping rate κ . Electrons can tunnel to and from the dot at tunneling rates Γ_a . Voltage drops, V_a , with respect to ϵ_0 are indicated. Reproduced with permission.^[105] Copyright 2019, American Physical Society. (c) Schematic diagram of the graphene-BN resonant tunneling transistor. Reproduced with permission.^[121] Copyright 2013, Springer Nature. (d) Device schematics of the resonant tunneling transistor with an exaggerated angle θ between two graphene layers (separated by an h-BN tunnel barrier shown in light blue). Both graphene layers are independently contacted by Cr/Au metallization (yellow). Reproduced with permission.^[122] Copyright 2014, Nature Publishing Group. (e) Schematic of the in-plane SET based on graphene-quantum-dots (GQDs). Reproduced with permission.^[130] Copyright 2019, Springer Nature. (f) Schematic view of the vertical van der Waals structure based on BP/alumina/BP. Reproduced with permission.^[131] Copyright 2020, Nature Publishing Group.

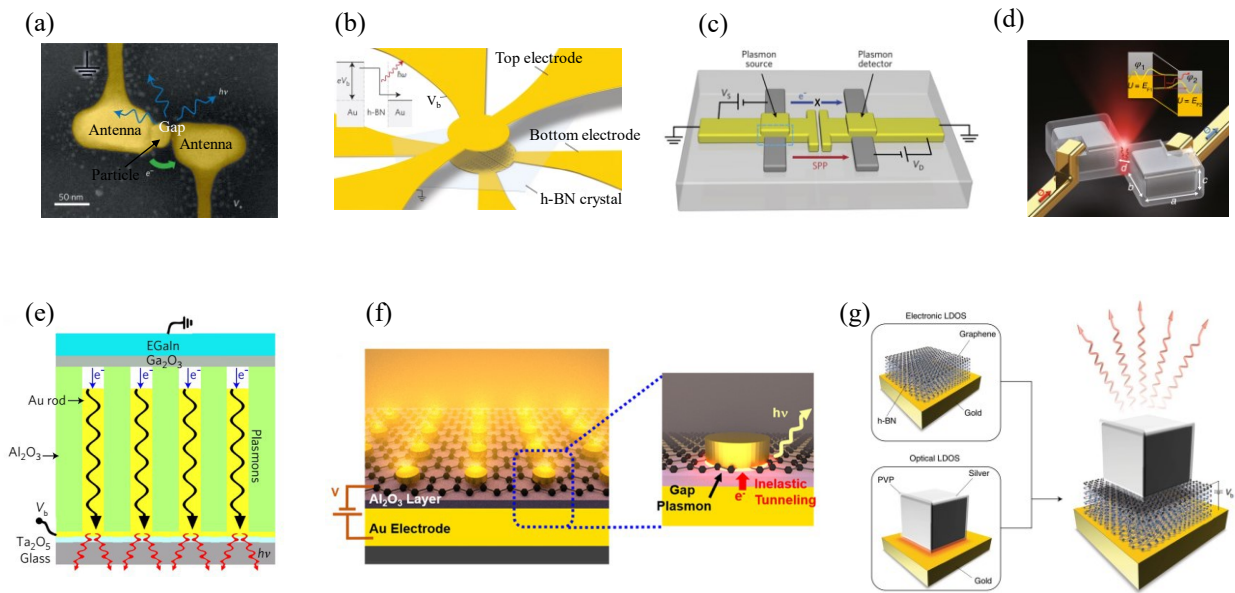


Figure 5. Representative inelastic tunneling devices. (a) Electron micrograph of a lateral tunneling device: an electrically connected single-crystalline gold nanoantenna loaded with a coated gold nanoparticle on a glass substrate. V_+ , applied voltage; e^- , electron flow; $h\nu$, light emission. Reproduced with permission.^[43] Copyright 2015, Nature Publishing Group. (b) Schematic illustration of metal-insulator-metal (MIM) tunneling devices. The devices consist of a vertical stack of segmented, nanostructured Au bottom electrodes, few-layer h-BN and a common Au top electrode. Inset: generation of a photon with energy $\hbar\omega$ by inelastic electron tunneling. Reproduced with permission.^[41] Copyright 2015, Nature Publishing Group. (c) Schematic illustration of a device consisting of two MIM tunneling junctions connected to a plasmonic waveguide. The left junction is the plasmon source and the right junction is the plasmon detector. Reproduced with permission.^[44] Copyright 2017, Nature Publishing Group. (d) Schematic diagram of a tunnel junction formed by two edge-to-edge Ag single-crystal cuboids encapsulated by a layer of polymer. The top inset shows that the photons are generated through inelastic electron tunneling. Here, E_{F1} and E_{F2} are the Fermi energies of the left and right Ag cubes, respectively. The device performance can be engineered by tuning the geometrical parameters of the tunnel junction including the gap size d , the size of the cuboids (a , b , c) and the curvature of the Ag cuboid edges. Reproduced with permission.^[42] Copyright 2018, Nature Publishing Group. (e) Schematic of the configuration of an electrically driven nanorod metamaterial based on metal-air-metal tunnel junctions. When a bias is applied between the EGaIn layer and Au nanorods, electrons tunnel across the junctions from occupied states in EGaIn to unoccupied states in Au. Reproduced with permission.^[45] Copyright 2018, Nature Publishing Group. (f) Schematic image of light emission from a nanoparticle array using a graphene tunnel junction (left) and underlying emission mechanism (right). A single plasmonic nanoparticle generates light when a voltage is applied across the tunnel barrier. The tunneling electrons lose their energy by exciting gap plasmons of the single nanoparticle, and the exciting gap plasmons decay into far-field radiation. Reproduced with permission.^[49]

Copyright 2018, American Chemical Society. (g) Illustration of a gold-few-layer h-BN-graphene van der Waals quantum tunneling (vdWQT) device, integrated with a (silver, PVP-coated) nanocube antenna. In this device configuration, the electronic LDOS is controlled by the hybrid vdWs heterostructure whereas the optical LDOS is governed by the nanocube antenna. Applying a voltage V_b across the insulating few-layer h-BN crystal results in antenna-mediated photon emission (wavy arrows) due to quantum tunneling. Reproduced with permission.^[50] Copyright 2019, Springer Nature.

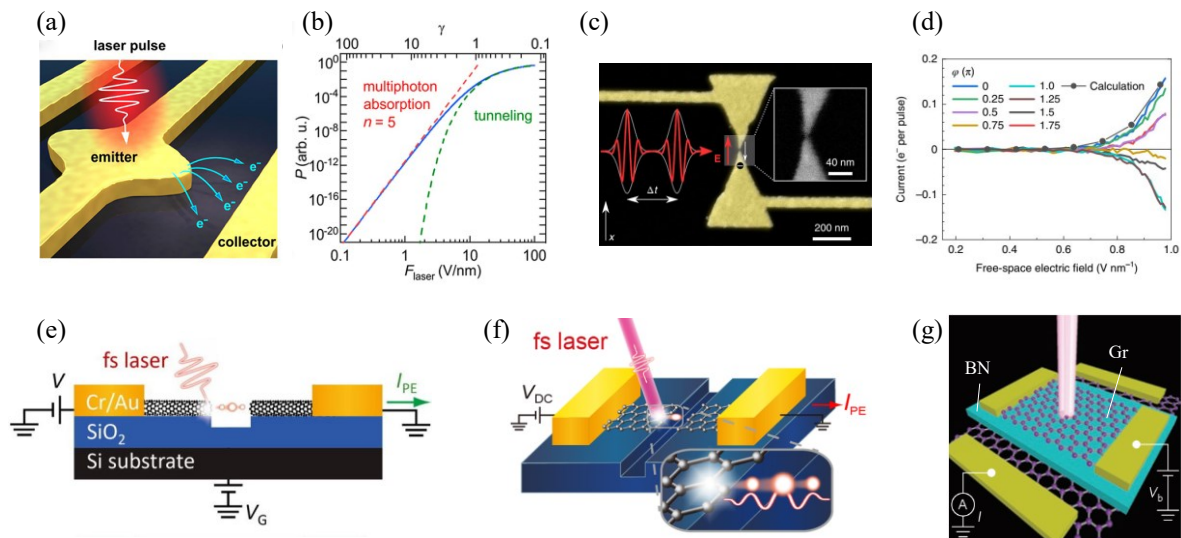


Figure 6. Representative optical-field-driven direct tunneling devices. (a) Sketch of a metallic tunneling junction with electrons being emitted after excitation with a femtosecond laser pulse (Laser energy: 0.9–1.3 eV, F_{laser} : 0.6 V/nm). (b) Electron emission probability as a function of the laser's optical field intensity F_{laser} as suggested by Keldysh Theory (blue line). The corresponding Keldysh parameter γ is displayed on the top axis. For a low F_{laser} , the Keldysh curve approaches the multiphoton absorption regime (red dashed line), whilst for a high F_{laser} , the Keldysh curve is approximated by an optical-field tunneling probability (green dashed line). (a–b) Reproduced with permission.^[158] Copyright 2019, American Chemical Society. (c) SEM image of a gold bow-tie antenna with two electric contacts. Two single-cycle laser pulses delayed by a time Δt are focused onto the nanogap. The red arrow indicates the positive direction of the electric field and the white arrow gives the corresponding direction of the electron transfer. Inset: Enlarged view of the gap region. (d) The pulse-averaged light-driven current induced as a function of free-space electric field amplitude of the laser pulses. The current is modulated sinusoidally with a phase ϕ that is directly related to the far-field CEP of the driving pulse $\phi = \text{CEP} + \delta$. (c–d) Reproduced with permission.^[154] Copyright 2019, Nature Publishing Group. (e) Schematic of femtosecond-laser-induced field emission in the SWNT nanogap device. Reproduced with permission.^[165] Copyright 2019, AIP Publishing. (f) Schematic of femtosecond-laser-induced field emission in a graphene nanogap tunneling device. Reproduced with permission.^[166] Copyright 2018, American Chemical Society. (g) Schematic of a Gr-BN-Gr device under optical excitation. Reproduced with permission.^[167] Copyright 2016, Nature Publishing Group.

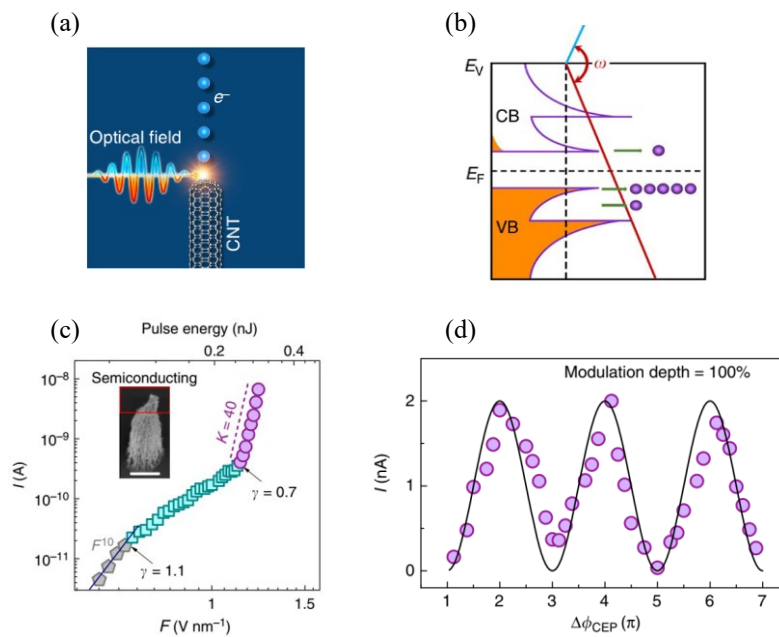


Figure 7. Extreme nonlinear strong-field photoemission from CNTs. (a) Diagram of optical-field emission (OFE) from CNT. Electrons (blue balls) are emitted from semiconducting CNT, driven by a negative half-cycled (red line) strong electromagnetic field of a femtosecond laser. (b) Diagram of transition into the valence band-dominated OFE (VB-OFE) that occurs at a relatively high optical-field strength. (c) I - F curve of aged CNT cluster in which the metallic tubes have been removed. Three different regimes of nonlinear behavior are observed: multiphoton photoemission (MPP) (gray pentagonal dots); conduction band-dominated OFE (CB-OFE) (green square dots); VB-OFE (purple circular dots). An extremely high slope of $K=40$ (dashed line) was observed. The inset shows the SEM image of the emitter. Scale bar is 2 μm . (d) The CEP-dependent photoemission current at a fixed laser intensity with a peak $F=1.3$ Vnm^{-1} together with a cosine fit (solid line). (a-d) Reproduced with permission.^[73] Copyright 2019, Springer Nature.

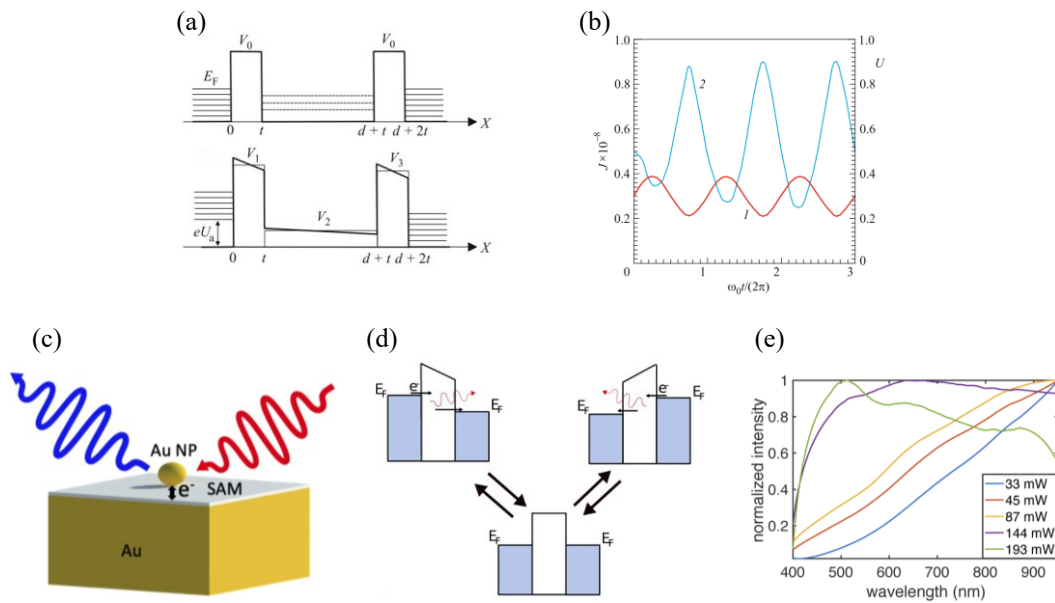


Figure 8. Other novel optical-field-driven tunneling devices. (a-b) Time-dependent resonant tunneling in a double-barrier diode structure. (a) Top: potential function profile for the symmetric double-barrier structure (the energy is measured from the bottom of the conduction band of the cathode). Bottom: its distortion induced by the voltage U_a applied to the anode (the energy is measured from the bottom of the conduction band of the anode). (b) Voltage U and current density J versus the dimensionless time $\tilde{t} = \omega_0 t / (2\pi)$. (a-b) Reproduced with permission.^[171] Copyright 2019, Springer Nature. (c-e) Light-induced inelastic tunneling emission. (c) Schematic of a metal nanoparticle on an ultraflat gold film covered with a self-assembled monolayer. An incident light pulse drives electron tunneling which emits a higher energy photon due to inelastic scattering. (d) Schematic of light-induced inelastic tunneling emission (LITE) effect resulting from the AC field of a femtosecond laser creating an oscillating bias voltage across the tunnel junction. The bias field is represented by a slope in the barrier potential. When the field induces tunneling, an upconverted photon can be emitted by inelastic scattering. (e) Emission spectra for four different average powers, showing the characteristic spectral shift of LITE. (c-e) Reproduced with permission.^[172] Copyright 2020, Optical Society of America.